Title: A temperature-inducible protein module for control of mammalian cell fate

Authors: William Benman[1#], Zikang Huang[1#], Pavan Iyengar[2], Delaney Wilde[1], Thomas R. Mumford[1], Lukasz J. Bugaj[1,3,4,*]

[#]equal contribution
*corresponding author

Affiliations:
[1]Department of Bioengineering, University of Pennsylvania, Philadelphia, PA, 19104, USA
[2]Department of Biophysics, University of Pennsylvania, Philadelphia, PA, 19104, USA
[3]Institute for Regenerative Medicine, University of Pennsylvania, Philadelphia, PA, 19104, USA
[4]Abramson Cancer Center, University of Pennsylvania, Philadelphia, PA, 19104, USA

Contact Information
bugaj@seas.upenn.edu

One-Sentence Summary: We introduce Melt, a protein whose activity can be toggled by a change in temperature of 3-4 degrees, and we demonstrate its ability to regulate a variety of protein and cell behaviors.

Abstract: Inducible protein switches are used throughout the biosciences to allow on-demand control of proteins in response to chemical or optical inputs. However, these inducers either cannot be controlled with precision in space and time or cannot be applied in optically dense settings, limiting their application in tissues and organisms. Here we introduce a protein module whose active state can be reversibly toggled with a small change in temperature, a stimulus that is both penetrant and dynamic. This protein, called Melt (Membrane localization through temperature), exists as a monomer in the cytoplasm at elevated temperatures but both oligomerizes and translocates to the plasma membrane when temperature is lowered. Using custom devices for rapid and high-throughput temperature control during live-cell microscopy, we find that the original Melt variant fully switches states between 28-32°C, and state changes can be observed within minutes of temperature changes. Melt was highly modular, permitting thermal control over diverse intracellular processes including signaling, proteolysis, and nuclear shuttling through straightforward end-to-end fusions with no further engineering. Melt was also highly tunable, giving rise to a library of Melt variants with switch point temperatures ranging from 30-40°C. The variants with higher switch points allowed control of molecular circuits between 37°C-41°C, a well-tolerated range for mammalian cells. Finally, Melt could thermally regulate important cell decisions over this range, including cytoskeletal rearrangement and apoptosis. Thus Melt represents a versatile thermogenetic module that provides straightforward, temperature-based, real-time control of mammalian cells with broad potential for biotechnology and biomedicine.

Main Text:

Inducible proteins provide a wealth of strategies for on-demand, remote control of cell behavior, for example using chemicals or light as inputs. These inputs trigger protein conformational changes that can regulate a vast array of downstream protein and cell behaviors in a modular manner. While chemical control requires delivery of a small molecule, light can be applied remotely and offers further benefits for precision in both space and time, as well as low cost of the inducer. There is tremendous potential to extend these benefits into more complex settings including in 3D cell and tissue models, in patients for control of cell therapy, or in dense bioreactors for bioproduction. However, optical control is limited in these more opaque settings because visible light cannot penetrate, for example scattering within millimeters of entering human tissue [1,2]. There is thus a need for alternative inducer strategies that couple the penetration of chemical induction with the spatiotemporal precision of optogenetics.

Temperature has gained recent interest as a dynamic and penetrant inducer [3–6]. Unlike light, temperature can be regulated tens of cm deep within tissue with sub-millimeter-scale precision using technologies like focused ultrasound that are already used in the clinic [7]. Furthermore, unlike either chemical- or light-induction, thermal-responsiveness could uniquely interface with an organism's own stimuli, setting the stage for engineered biological systems that autonomously detect and respond to physiological temperature cues, for example fevers or inflammation.

The widespread adoption of chemo- and opto-genetic proteins was enabled by the identification protein domains that undergo stereotyped and consistent changes in response to small molecules or light. However, remarkably few analogous temperature-sensing modules have been described. Endogenous heat shock promoters have been used for thermal control of transcription, including to induce tumor clearance by engineered cells [4,8,9]. However heat shock promoters can respond to non-thermal stimuli [10–12], and thermal response profiles cannot be readily tuned because they depend on the cell's repertoire of heat shock factor proteins. Moreover, many desirable cell behaviors (e.g. migration, proliferation, survival/death) cannot be easily controlled at the transcriptional level. At the post-translational level, temperature-sensitive (Ts) mutants are protein variants that denature at elevated temperatures [13–15]. However, Ts mutations are generally not modular or reversible and must be laboriously validated for each individual target. The TlpA protein from *Salmonella* forms thermolabile dimers[16] and underlies existing thermosensitive engineered proteins, including a temperature-controlled dimerization module [17]. However TlpA-based dimers are large (~600-700 amino acids in combined size), and may be limited by the need for stoichiometric tuning between the two components. The identification of distinct temperature-responsive proteins, especially with functions beyond dimerization, is critical for broad development and application of thermogenetic approaches.

Here we introduce a unique thermoresponsive protein module called Melt (Membrane localization using temperature), which we derived from the naturally light- and temperature-sensitive BcLOV4 protein [18]. Melt is a single protein that clusters and binds the plasma membrane at low temperatures but dissociates and declusters upon heating. Using live-cell

imaging coupled with custom devices for precise temperature control in 96-well plates, we found that Melt could be toggled between these two states rapidly and reversibly, with observable membrane dissociation and recovery within 10s of minutes. The Melt approach was highly modular, allowing thermal control of diverse processes including EGFR and Ras signaling, TEVp proteolysis, and subcellular localization through simple end-to-end fusion of the appropriate effectors. We then tuned Melt to increase its switchpoint temperature above the native 30°C. Such tuning resulted in Melt variants that operated with switch point temperatures between 30-40°C, including ones that bound the membrane at 37°C and fully dissociated at 39°C or 42°C, temperature ranges suitable for downstream application in mammalian tissues. These variants controlled multiple post-translational circuits between 37°C and 42°C and could regulate important cell-level behaviors including cytoskeletal reorganization and apoptosis. Thus Melt offers a straightforward, tunable, and broadly applicable platform for endowing thermal control across a wide range of molecular and cellular behaviors.

RESULTS

BcLOV4 is a modular optogenetic protein that natively responds to both blue light and temperature [18,19] (**Figure 1A**). Light stimulation triggers its clustering and translocation from the cytoplasm to the plasma membrane, where it binds anionic phospholipids [19,20]. However, its persistence at the membrane requires both continued light and a permissive temperature. At temperatures above 29°C, membrane binding is transient; BcLOV4 binds but then returns to the cytoplasm (**Figure 1A-C**) at a rate that increases with temperature [18]. Our previous report found that, once dissociated due to elevated temperatures, BcLOV4 remains in the cytoplasm and no longer responds to light stimuli [18]. However, we found that lowering temperature below the 29°C threshold reversed this inactivation and restored light-dependent membrane localization (**Figure 1C**). Thus, temperature alone could be used to toggle the localization of BcLOV4 given the continued presence of blue light.

We sought to harness this thermal responsiveness to generate a protein actuator that responded only to temperature. We reasoned that a BcLOV4 variant with a point mutation that mimicked the “lit” state would localize to the membrane independent of light status but should retain thermal sensitivity (**Figure 1D**). We thus introduced a Q356N mutation that disrupts the dark-state interaction between the Jα helix and the core of the LOV domain [19,21]. When expressed in HEK 293T cells at 37°C, BcLOV(Q356N)-mCh appeared mostly cytoplasmic and did not respond to blue light (**Figure 1E-G**). Strikingly, shifting the temperature from 37°C to 25°C triggered an accumulation of the protein at the plasma membrane, where increasing accumulation was observed within minutes and continued over the next three hours (**Figure 1D-H**). Membrane localization of Melt was often accompanied by visible clustering at the membrane, consistent with our prior findings that clustering and membrane-binding are interlinked properties of BcLOV4 [20] (**Fig 1B,C,F).** Conversely, the native photosensitive BcLOV4 did not accumulate at the membrane in response to temperature in the absence of light (**Figure 1G,H**). Thus, BcLOV4(Q356N)—henceforth referred to as Melt (Membrane localization using temperature)—is a light-insensitive protein whose subcellular localization can be regulated solely by temperature.

We next sought to comprehensively characterize the thermal response properties of Melt, including how the amplitude and kinetics of membrane dissociation/reassociation varied with time and temperature. To systematically explore this large parameter space, we developed a device that allowed rapid, programmable heating of individual wells of 96-well plates. This device—the thermoPlate—has 96 pairs of thermistors arrayed in the format of a standard 96-well plate (**Figure 2A**). One thermistor serves as a miniature immersion heater (heater, **Figure 2B,C**) that heats the medium through resistive heating, while the second acts as a thermometer (reader, **Figure 2B,C**) that measures the temperature of the medium in a well. The heater and reader implement proportional-integral-derivative (PID) feedback control, which maintains a pre-defined temperature profile over even day-long experiments (**Figure 2D**). Because the thermoPlate has a thin profile and is positioned above a 96-well plate, it allows simultaneous live-cell imaging of the sample using an inverted microscope.

We first used multiplexed temperature control to measure steady-state Melt membrane association over a range of temperatures after 24 hrs of heating (**Figure 2E**). Membrane association was maximal at 27°C and minimal at 32°C, and reached 50% of this range at ~30°C, which we assign as its switch temperature. The thermoPlate also permits observation of fast thermal response dynamics by allowing rapid temperature changes (e.g. 10 degrees heating in 2.5 mins, 10 degrees cooling in 6 minutes, **Figure 2F**). By toggling temperature between 27 and 37, we could demonstrate reversible membrane binding and dissociation over multiple cycles (**Figure 2G,H, Supplementary Movie 1**). For full details on membrane binding quantification, see **Figure S1 and Methods.**

We next examined the kinetics of Melt translocation to and from the membrane. Dissociation kinetics increased with higher temperatures (**Figure 2I**). Notably, although steady-state membrane association was unchanged above 32°C (**Figure 2E**), the rate with which Melt reached this steady state level continued to increase with temperature (note the higher decay rate at 34°C and 37°C relative to 32°C, (**Figure 2I**). Reassociation kinetics depended on the thermal stimulation history. Samples that were stimulated at higher temperatures showed a lower degree of reversibility (**Figure 2J**). Reversibility was also a function of the duration of prior stimulation. Although dissociation after 30 min of heating at 37°C was fully reversible, longer stimulation led to smaller degrees of reversion (**Figure 2K**). Collectively, these data suggest that Melt is a thermoswitch that operates tunably and reversibly within a 27-32°C range, but whose reversibility is a function of the magnitude of its prior stimulation.

We explored the potential of Melt to control molecular circuits in mammalian cells in response to temperature changes. Recruitment of cargo to/from the membrane is a powerful mode of post-translational control, including for cell signaling [22]. We first targeted signaling through the Ras-Erk pathway, a central regulator of cell growth and cancer. We generated an end-to-end fusion of Melt to the catalytic domain of the Ras activator SOS2 [23], an architecture that previously allowed potent stimulation of Ras signaling using optogenetic BcLOV4 [18]. We expressed this construct (meltSOS) in HEK 293T cells and measured Erk activation upon changing temperature from 37°C to 27°C (**Fig 3A**). Active Erk (phospho-Erk, or ppErk) could be observed even within 5 minutes of temperature change to 27°C and continued to rise until its plateau at 30 mins (**Fig 3B,C**). Conversely, shifting temperature from 27°C back to 37°C

resulted in measurable signal decrease within 5 min and full decay within 30 mins (**Figure 3B,C**), comparable to the kinetics of thermal inactivation during optogenetic stimulation of BcLOV-SOS [18].

Separately, we tested whether we could leverage the clustering of Melt for control of signaling from the receptor level. We generated a fusion of Melt to the intracellular domain of the epidermal growth factor receptor (EGFR) (**Figure 3D**). EGFR is a receptor tyrosine kinase with important roles in development and tumorigenesis and stimulates intracellular signaling through multiple pathways, including Ras-Erk [24]. Importantly, both membrane recruitment and clustering of the EGFR intracellular domain are required for its activation [20,25]. In cells expressing meltEGFR, lowering the temperature from 37°C to 27°C activated strong Erk signaling within 10 minutes, and reversion to 37°C caused signal decay within 5 minutes, with full decay within 30-60 mins (**Figure 3E,F**). Thus, the inducible membrane recruitment and clustering of Melt can be used for rapid, potent, and reversible thermal control of signaling in a modular fashion.

When Melt activates proteins at the membrane, it operates as a heat-OFF system. We next examined whether Melt could also implement a heat-ON system by coupling membrane translocation to negative regulation. Proteases can negatively regulate their targets through protein cleavage in both natural and synthetic systems [26–28]. We thus tested whether Melt could regulate proteolysis at the membrane. We fused Melt to the viral TEV protease (meltTEVp) and we measured whether its membrane recruitment could trigger a membrane-associated reporter of TEVp activity, FlipGFP [29] (FlipGFP-CAAX). FlipGFP is non-fluorescent until proteolytic cleavage allows proper folding and maturation of the chromophore (**Figure 3G**). Cells that expressed meltTEVp and FlipGFP-CAAX showed minimal levels of fluorescence when cultured at 37°C, similar to cells that expressed FlipGFP-CAAX and cytoplasmic TEVp or FlipGFP-CAAX alone. However, culturing meltTEVp cells at lower temperatures for 24 hours increased FlipGFP fluorescence, with fluorescence increasing monotonically with decreasing temperature, whereas cells expressing cytoplasmic TEVp remained at baseline fluorescence (**Figure 3H,I, Figure S2**). Thus, Melt can implement thermal control of proteolysis, providing one method by which it could control downstream circuits as a heat-ON switch.

A second way to convert Melt to heat-ON is to regulate its subcellular compartmentalization. Here, the plasma membrane would sequester Melt, and heat would release sequestration and allow translocation to a separate compartment where it could perform a desired function. As a proof of concept, we engineered Melt to regulate nuclear localization by fusing it to sequences that facilitate nuclear import and export (**Figure 3J**). We tested several combinations of nuclear localization sequences (NLS) and nuclear export sequences (NES) to optimize the relative strengths of import and export (**Figure S3**). Melt fused to the SV40 NLS [30] and the Stradα NES [31] showed strong membrane binding and nuclear exclusion at 27°C and nuclear enrichment when heated to 37°C (**Figure 3K,L, SMovie 2**). This construct could be dynamically shuttled to and from the nucleus through repeated rounds of heating and cooling. By contrast, Melt without NLS/NES showed no nuclear accumulation upon heating (**Figure**

3K,L). Collectively, our results show that Melt can be applied to control a variety of molecular events, in either heat-ON or heat-OFF configuration, in a straightforward and modular manner.

The utility of Melt in mammals will depend on its ability to induce a strong change in localization in response to temperature, as well as on its ability to operate within a mammalian temperature range (37-42°C). We thus sought to tune these properties. To increase the magnitude of membrane translocation, we tested whether short polybasic (PB) peptides could strengthen the electrostatic molecular interactions that mediate BcLOV4 membrane binding (**Figure 4A,B)** [19,32]. We chose two well-characterized PB domains from the STIM1 and Rit proteins, which can enhance membrane-binding of unrelated proteins [33]. End-to-end fusions of Melt to the STIM, tandem STIM (STIM2X), or Rit domains all increased the magnitude of membrane binding at 27°C, in increasing order of strength (**Figure 4C,D**). Kinetic analysis showed that PB domains did not change the rate of Melt dissociation, although some changes in reassociation kinetics were observed (**Figure S4**).

Although PB domains provided a large increase in steady-state membrane binding at 27°C, they provided only a mild increase in thermal switch point to ~32°C, only 1-2 degrees higher than the original Melt (**Figure 4D).** We achieved a more substantial increase through the fortuitous discovery that the C293 residue plays an important role in defining the Melt thermal response. In wt BcLOV4, C293 is thought to form a light-dependent bond with a flavin mononucleotide cofactor that underlies the BcLOV4 photoresponse [19]. Although Melt translocation did not respond to light (**Figure 1G)**, introduction of a C293A mutation dramatically increased its membrane association not only at 27°C, but also at 37°C where the original Melt was fully dissociated **(Figure 4F,G, Fig S5**). As before, addition of the STIM PB domain further increased membrane association strength at these higher temperatures. Importantly, both C293A variants retained temperature sensitivity and fully dissociated from the membrane at 41-42°C, with a thermal switch point of 36.5 and 39.5°C for the C293A and C293A/STIM variants, respectively (**Figure 4H, Figure S6**). Because these Melt variants can exist in one state at 37°C and another at 41/42°C, they are thus both potentially suitable for actuation within mammalian tissues, with distinct levels of membrane binding and dynamic range that could each be optimal for certain applications. These variants also included a truncation of 96 amino acids from the N-terminal of BcLOV4, which we found expendable, consistent with previous results [19]. Collectively, our work presents four Melt variants with a range of thermal switch points between 30°C and 40°C, covering temperatures suitable for actuation of a broad range animal cells. We adopted a nomenclature for these variants that reflects these switch-points: Melt-30, Melt-32, Melt-37, and Melt-40.

We tested the ability of the higher switch-point Melt variants to actuate post-translational events between 37 and 42°C. meltEGFR driven by Melt-37 showed strong Erk activation at 37°C and only baseline levels at 40-41°C (**Figure 4I,J**). Erk activity could be stimulated repeatedly over multiple heating/cooling cycles as indicated by the ErkKTR biosensor, which translocates from the nucleus to the cytoplasm upon Erk activation (**Figure 4K,L, Supplementary Movie 3**) [34]. meltSOS-37 could also stimulate Erk activity but only at <~37°C,

potentially reflecting a requirement for higher levels of membrane translocation relative to meltEGFR [20] (**Figure S7)**.

Melt-37/40 could also regulate behaviors that allowed its inversion to a heat-ON signal. Melt-40 fused to TEVp showed strong proteolysis and FlipGFP activation at 37°C, with markedly reduced activity at 41°C (**Figure 4M-O**). Melt-37 also regulated proteolysis but only induced fluorescence at or below 35°C, and fluorescence fell to near baseline at 37°C (**Figure S8**). These results further highlight that although the general thermal response properties are dictated by the specific Melt variant, the precise thermal switch point of the downstream process can be influenced by the specific fusion partner or the downstream process itself. Melt-40 also regulated membrane-to-nuclear translocation within the well-tolerated 37-41°C temperature range (**Figure 4P**). Fusion to a C-terminal SV40 NLS and Stradα NES allowed strong membrane sequestration at 37°C, and fluorescence became enriched in the nucleus upon heating to 41°C (**Figure 4Q,R**). As before, translocation was partially reversible on the timescales tested and could be cycled through repeated rounds of heating and cooling (**Figure 4Q,R, Supplementary Movie 4**).

We then asked whether Melt variants could be used to regulate cellular-level behaviors at and above 37°C. We first sought to control cell shape changes through the control of actin polymerization. We fused Melt-37 to the DH-PH domain of Intersectin1 (meltITSN1-37), an activator of the Rho GTPase Cdc42 that has previously been actuated through optogenetic recruitment [35], including with BcLOV4 [36,37] (**Figure 5A**). When cooled from 41°C to 37°C, HEK 293T cells expressing meltITSN1 showed rapid and dramatic expansion of lamellipodia and cell size, consistent with Cdc42 activation [38] (**Figure 5B**). Changes in cell shape could be reversed and re-stimulated over multiple cycles of cooling and heating (**Figure 5C**), showing similar magnitude of shape change in each round (**Figure 5D, S9, Supplementary Movie 5**). By comparison, temperature changes had no effect on cell shape in cells that expressed Melt-37 without the ITSN1 DH-PH domain.

As a second example, we asked if Melt could be used for thermal control of cell death. Cell death can be achieved by regulated clustering of effector domains of caspase proteins [39]. We reasoned that differential clustering of Melt at different temperatures could be leveraged to regulate caspase activity and cell death. We fused Melt-37 to the effector domain of caspase-1 (meltCasp1-37, **Figure 5E**), and we measured cell death upon changes in temperature (**Figure 5F**). While cells expressing meltCasp1-37 appeared unperturbed at 38°C, transition to 34°C led to morphological changes within minutes, followed within hours by blebbing and cell death, indicated by both morphology and AnnexinV staining (**Figure 5G,H, Supplementary Movie 6**). ThermoPlate scanning coupled with live cell imaging of AnnexinV allowed us to observe death induction with 1°C resolution, revealing cell death induction even when shifting temperature by only 1°C (from 38°C-37°C), and the magnitude of cell death increased with larger temperature shifts (**Figure 5I,J**). No death was measured in cells expressing Melt-37 without the caspase effector.

Finally, a potential concern for using heat as a stimulus is that heat is a known stressor and could adversely affect cell functions. However, we observed no molecular or functional effects of either the short- or long-term heat profiles used throughout our studies in mammalian cells. Stress granules (SGs), a known consequence of heat-stress[40,41], were not observed at 41°C or below in HEK 293T cells, the operating temperatures for the highest switch-point Melt variants (**Figure S10A,B)**. By contrast, SGs could be detected at 42°C in ~1-5% of cells, and at 43°C all cells showed strong SG formation. Of note, existing strategies for thermal induction (e.g. heat shock promoters, thermomers) are typically stimulated with 42°C[4,8,9,17], at the cusp of this non-linear heat-induced SG response (**Figure S10B**). We also measured cell proliferation to investigate potential integration of low-level heat stress during multi-hour heating (**Figure S10C)**. Again, regardless of temperature between 37-42°C, we measured no difference in the fraction of cells with high phospho-Rb levels, a marker of proliferation, or of total cell counts through 24 hr of heating (**Figure S10D-F)**.

In sum, membrane binding and clustering of Melt variants can be harnessed to control a diverse array of protein and cell behavior over a broad range of temperatures, including those relevant for mammalian cells, which can be thermally controlled by Melt with a larger buffer from potential heat stress compared to the few alternative approaches.

DISCUSSION

Here we have described a modular and tunable protein that permits thermal control over a range of molecular and cell-level behaviors. By locking the naturally light- and temperature-sensitive BcLOV4 into its “lit” state, we generated the purely thermoresponsive Melt whose membrane association and clustering can be regulated with a small temperature change (<4°C). Tuning this thermal response further allowed us to generate multiple variants (Melt-30/32/37/40) whose activation switch points could be shifted within the 30-40°C range. These variants allowed temperature-inducible control of signaling, proteolysis, and subcellular localization, including between 37°C-42°C, a critical range for thermal control within mammals. Finally, we showed that Melt can provide thermal control over cell-level behaviors by changing cell size/shape and cell death.

Our engineering efforts provide insight into how the wt BcLOV4 protein senses both light and temperature. Successful isolation of the BcLOV4 thermal response from its light response confirms the distinct molecular nature of these two behaviors, as previously speculated [18]. At the same time, the light and temperature responses are closely linked, since mutation of the C293 residue in the LOV domain, which mediates photo-responsiveness, dramatically shifted the thermal switchpoint of Melt (**Figure 4E**). Further mechanistic and structural work will be required to fully understand the molecular basis for BcLOV thermal sensitivity, potentially allowing optimization of Melt properties including speed of response and degree of reversibility, and will shed light on how the photosensing and thermosensing elements of BcLOV4 interact. These latter studies will additionally provide insight for how to engineer novel multi-input proteins that can perform complex logic in response to user-defined stimuli.

Our work also introduces the thermoPlate, a device for independent reading and writing of temperature within each well of a 96-well plate. The thermoPlate allows rapid (~minutes) and dynamic heating and cooling of samples, which allowed quantitative systematic characterization of the kinetics and reversibility of multiple Melt variants. Importantly, multiplexed control of temperature with the thermoPlate is constrained by thermal diffusion, since a hot well will influence the temperature in neighboring wells. However, with careful definition of sample position within a plate, choice of ambient temperature, and PID feedback control, the challenges of thermal diffusion can be overcome. The thermoPlate is fully open source and can be assembled in under 6 hours for ~$400. We anticipate this device will be highly enabling for any use case where multiplexed or dynamic thermal control is required.

Multiplexed control of sample temperature allowed us to systematically characterize new Melt variants, ultimately resulting in variants with switch-points ranging from 30-40°C. Because BcLOV4 works in mammalian cells but also in systems that are cultured at lower temperatures like yeast, flies, zebrafish, and ciona, [18,19,36,42–44], we anticipate that all Melt variants will find use across these and similar settings. Our work also highlights the utility of having multiple variants in hand to optimize specific downstream applications. We found on multiple occasions that the precise thermal response profiles depended not only on the specific Melt variant but also on the downstream process under control, requiring empirical validation for each use case and biological context. Optimization can be performed by testing other Melt variants, or by generating new ones through additional modifications (e.g. polybasic domains) or mutations.

Melt dramatically expands the range of molecular and cellular events that can be controlled by temperature, and in mammalian cells allows thermal control with lower potential for heat stress relative to the few existing approaches. Melt provides an orthogonal input control on biological systems that can be used in conjunction with—or instead of—existing technologies based on light or chemicals, promising to expand the sophistication and reach of biological control with broad potential for biotechnology and biomedicine.

References and Notes

1. Ntziachristos, V. Going deeper than microscopy: the optical imaging frontier in biology. *Nat. Methods* **7**, 603–614 (2010).
2. Ash, C., Dubec, M., Donne, K. & Bashford, T. Effect of wavelength and beam width on penetration in light-tissue interaction using computational methods. *Lasers Med. Sci.* **32**, 1909–1918 (2017).
3. Piraner, D. I. *et al.* Going Deeper: Biomolecular Tools for Acoustic and Magnetic Imaging and Control of Cellular Function. *Biochemistry* **56**, 5202–5209 (2017).
4. Miller, I. C. *et al.* Enhanced intratumoural activity of CAR T cells engineered to produce immunomodulators under photothermal control. *Nat Biomed Eng* **5**, 1348–1359 (2021).
5. Ermakova, Y. G. *et al.* Thermogenetic control of Ca2+ levels in cells and tissues. *bioRxiv* 2023.03.22.533774 (2023) doi:10.1101/2023.03.22.533774.
6. Corbett, D. C. *et al.* Thermofluidic heat exchangers for actuation of transcription in artificial tissues. *Sci Adv* **6**, (2020).
7. ter Haar, >gail & Coussios, C. High intensity focused ultrasound: Physical principles and devices. *Int. J. Hyperthermia* **23**, 89–104 (2007).
8. Abedi, M. H., Lee, J., Piraner, D. I. & Shapiro, M. G. Thermal Control of Engineered T-cells. *ACS Synth. Biol.* **9**, 1941–1950 (2020).
9. Wu, Y. *et al.* Control of the activity of CAR-T cells within tumours via focused ultrasound. *Nat Biomed Eng* **5**, 1336–1347 (2021).
10. Morimoto, R. I. Cells in stress: transcriptional activation of heat shock genes. *Science* **259**, 1409–1410 (1993).
11. Feder, M. E. & Hofmann, G. E. HEAT-SHOCK PROTEINS, MOLECULAR CHAPERONES, AND THE STRESS RESPONSE: Evolutionary and Ecological Physiology. (2003) doi:10.1146/annurev.physiol.61.1.243.
12. Akerfelt, M., Morimoto, R. I. & Sistonen, L. Heat shock factors: integrators of cell stress, development and lifespan. *Nat. Rev. Mol. Cell Biol.* **11**, 545–555 (2010).
13. Horowitz, N. H. Biochemical Genetics of Neurospora. in *Advances in Genetics* (ed. Demerec, M.) vol. 3 33–71 (Academic Press, 1950).
14. Talavera, A. & Basilico, C. Temperature sensitive mutants of BHK cells affected in cell cycle progression. *J. Cell. Physiol.* **92**, 425–436 (1977).
15. Varadarajan, R., Nagarajaram, H. A. & Ramakrishnan, C. A procedure for the prediction of temperature-sensitive mutants of a globular protein based solely on the amino acid sequence. *Proc. Natl. Acad. Sci. U. S. A.* **93**, 13908–13913 (1996).
16. Hurme, R., Berndt, K. D., Normark, S. J. & Rhen, M. A proteinaceous gene regulatory thermometer in Salmonella. *Cell* **90**, 55–64 (1997).
17. Piraner, D. I., Wu, Y. & Shapiro, M. G. Modular Thermal Control of Protein Dimerization. *ACS Synth. Biol.* **8**, 2256–2262 (2019).
18. Benman, W. *et al.* Temperature-responsive optogenetic probes of cell signaling. *Nat. Chem. Biol.* **18**, 152–160 (2022).
19. Glantz, S. T. *et al.* Directly light-regulated binding of RGS-LOV photoreceptors to anionic membrane phospholipids. *Proc. Natl. Acad. Sci. U. S. A.* **115**, E7720–E7727 (2018).
20. Pal, A. A., Benman, W., Mumford, T. R., Chow, B. Y. & Bugaj, L. J. Optogenetic clustering and membrane translocation of the BcLOV4 photoreceptor. *bioRxiv* 2022.12.12.520131 (2022) doi:10.1101/2022.12.12.520131.
21. Harper, S. M., Neil, L. C. & Gardner, K. H. Structural basis of a phototropin light switch. *Science* **301**, 1541–1544 (2003).
22. Grecco, H. E., Schmick, M. & Bastiaens, P. I. H. Signaling from the living plasma membrane. *Cell* **144**, 897–909 (2011).
23. Toettcher, J. E., Weiner, O. D. & Lim, W. A. Using optogenetics to interrogate the dynamic control of signal transmission by the Ras/Erk module. *Cell* **155**, 1422–1434 (2013).

24. Citri, A. & Yarden, Y. EGF-ERBB signalling: towards the systems level. *Nat. Rev. Mol. Cell Biol.* **7**, 505–516 (2006).
25. Liang, S. I. *et al.* Phosphorylated EGFR Dimers Are Not Sufficient to Activate Ras. *Cell Rep.* **22**, 2593–2600 (2018).
26. Chung, H. K. *et al.* A compact synthetic pathway rewires cancer signaling to therapeutic effector release. *Science* **364**, (2019).
27. Gao, X. J., Chong, L. S., Kim, M. S. & Elowitz, M. B. Programmable protein circuits in living cells. *Science* **361**, 1252–1258 (2018).
28. Sanchez, M. I. & Ting, A. Y. Directed evolution improves the catalytic efficiency of TEV protease. *Nat. Methods* **17**, 167–174 (2020).
29. Zhang, Q. *et al.* Designing a Green Fluorogenic Protease Reporter by Flipping a Beta Strand of GFP for Imaging Apoptosis in Animals. *J. Am. Chem. Soc.* **141**, 4526–4530 (2019).
30. Collas, P. & Aleström, P. Nuclear localization signal of SV40 T antigen directs import of plasmid DNA into sea urchin male pronuclei in vitro. *Mol. Reprod. Dev.* **45**, 431–438 (1996).
31. Dorfman, J. & Macara, I. G. STRADalpha regulates LKB1 localization by blocking access to importin-alpha, and by association with Crm1 and exportin-7. *Mol. Biol. Cell* **19**, 1614–1626 (2008).
32. Heo, W. D. *et al.* PI(3,4,5)P3 and PI(4,5)P2 lipids target proteins with polybasic clusters to the plasma membrane. *Science* **314**, 1458–1461 (2006).
33. He, L. *et al.* Optical control of membrane tethering and interorganellar communication at nanoscales. *Chem. Sci.* **8**, 5275–5281 (2017).
34. Regot, S., Hughey, J. J., Bajar, B. T., Carrasco, S. & Covert, M. W. High-Sensitivity Measurements of Multiple Kinase Activities in Live Single Cells. *Cell* **157**, 1724–1734 (2014).
35. Levskaya, A., Weiner, O. D., Lim, W. A. & Voigt, C. A. Spatiotemporal control of cell signalling using a light-switchable protein interaction. *Nature* **461**, 997–1001 (2009).
36. Berlew, E. E. *et al.* Designing Single-Component Optogenetic Membrane Recruitment Systems: The Rho-Family GTPase Signaling Toolbox. *ACS Synth. Biol.* **11**, 515–521 (2022).
37. Hannanta-Anan, P., Glantz, S. T. & Chow, B. Y. Optically inducible membrane recruitment and signaling systems. *Curr. Opin. Struct. Biol.* **57**, 84–92 (2019).
38. Nobes, C. D. & Hall, A. Rho, rac, and cdc42 GTPases regulate the assembly of multimolecular focal complexes associated with actin stress fibers, lamellipodia, and filopodia. *Cell* **81**, 53–62 (1995).
39. Shkarina, K. *et al.* Optogenetic activators of apoptosis, necroptosis, and pyroptosis. *J. Cell Biol.* **221**, (2022).
40. Gallouzi, I. E. *et al.* HuR binding to cytoplasmic mRNA is perturbed by heat shock. *Proc. Natl. Acad. Sci. U. S. A.* **97**, 3073–3078 (2000).
41. Kedersha, N. L., Gupta, M., Li, W., Miller, I. & Anderson, P. RNA-binding proteins Tia-1 and tiar link the phosphorylation of eIF-2α to the assembly of mammalian stress granules. *J. Cell Biol.* **147**, 1431–1442 (1999).
42. Berlew, E. E. *et al.* Single-component optogenetic tools for inducible RhoA GTPase signaling. *Advanced Biology* 2100810 (2021).
43. Berlew, E. E., Kuznetsov, I. A., Yamada, K., Bugaj, L. J. & Chow, B. Y. Optogenetic Rac1 engineered from membrane lipid-binding RGS-LOV for inducible lamellipodia formation. *Photochem. Photobiol. Sci.* (2020) doi:10.1039/c9pp00434c.
44. Qiao, J., Peng, H. & Dong, B. Development and Application of an Optogenetic Manipulation System to Suppress Actomyosin Activity in Ciona Epidermis. *Int. J. Mol. Sci.* **24**, (2023).
45. Wang, W. *et al.* A light- and calcium-gated transcription factor for imaging and manipulating activated neurons. *Nat. Biotechnol.* **35**, 864–871 (2017).

46. Tidyr. https://tidyr.tidyverse.org/.
47. Wickham, H. ggplot2. *WIREs Computational Statistics* **3**, 180–185 (2011).
48. Legland, D., Arganda-Carreras, I. & Andrey, P. MorphoLibJ: integrated library and plugins for mathematical morphology with ImageJ. *Bioinformatics* **32**, 3532–3534 (2016).

Acknowledgements:

We thank Erin Berlew and Brian Chow for helpful discussions on BcLOV4 activity and for plasmids encoding BcLOV(Q356N) and BcLOV-ITSN1, and Alex Hughes and Matthew Good for helpful comments on the manuscript. We also thank the Penn Cytomics and Cell Sorting Shared Resource Laboratory for assistance with cell sorting. This work was supported by funding from the National Institutes of Health (R35GM138211 for L.J.B), the National Science Foundation (Graduate Research Fellowship Program to W.B., CAREER 2145699 to L.J.B.), and the Penn Center for Precision Engineering for Health. Cell sorting was performed on a BD FACSAria Fusion that was obtained through NIH S10 1S10OD026986.

Author Contributions

W.B. and L.J.B. conceived the study to generate Melt and downstream applications and to develop the thermoPlate. W.B. generated Melt and its integration into molecular circuits. Z.H. discovered and characterized thermostable Melt variants, which were then integrated into circuits by Z.H. and W.B. W.B. developed and validated the thermoPlate. D.W. and T.R.M. validated cluster-induced cell killing. W.B., Z.H., and P.I. performed and analyzed all experiments. L.J.B. supervised the work. W.B., Z.H., and L.J.B. wrote the manuscript and made figures, with editing from all authors.

List of Supplementary Materials

Materials and Methods.
Supplementary Figures 1-10.
Supplementary Movie Captions 1-6.

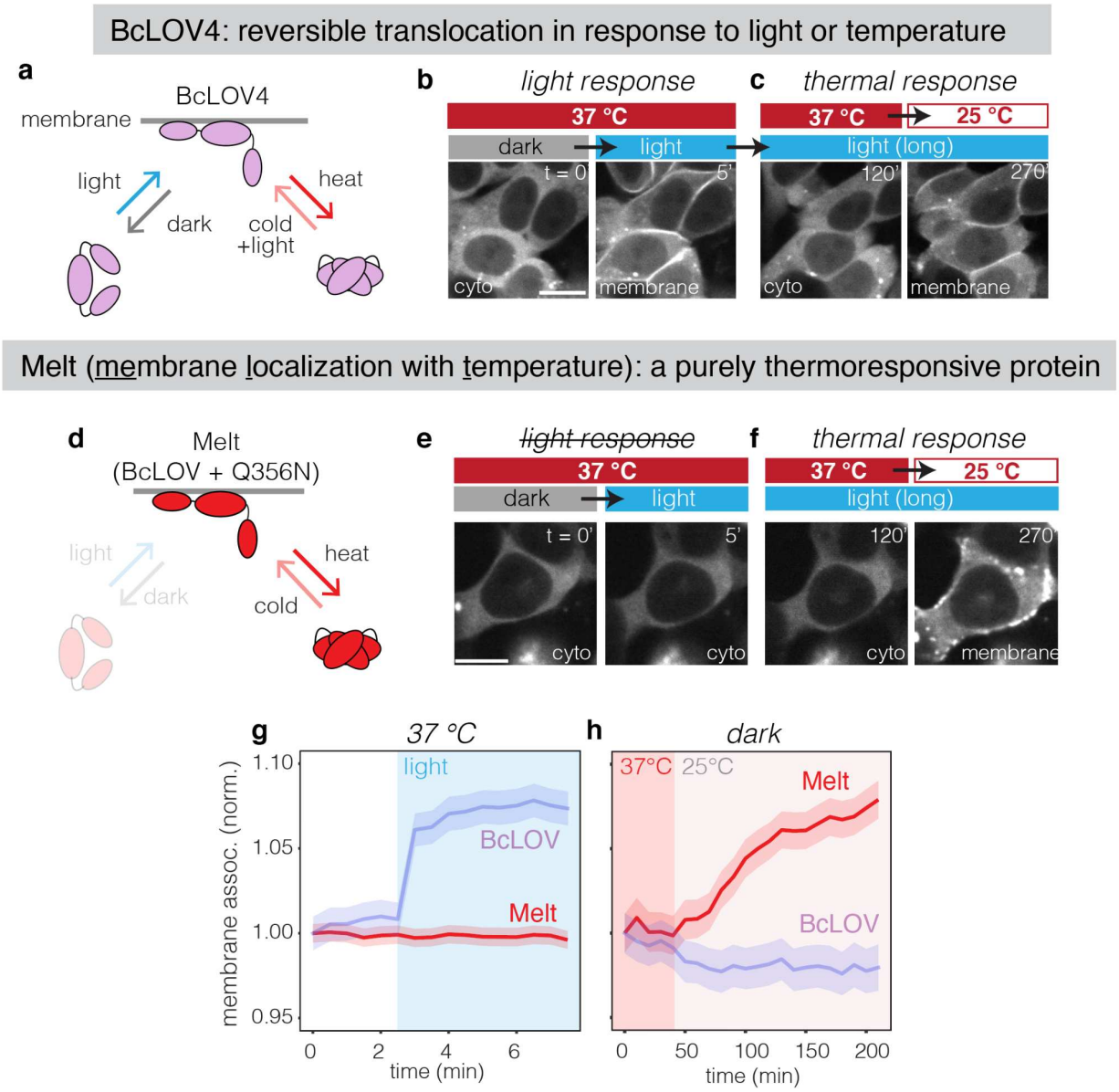

Fig. 1: Harnessing BcLOV4 thermosensitivity to generate a purely temperature-inducible protein. A) Schematic of BcLOV4, a naturally light- and temperature-responsive protein. BcLOV4 translocates to the membrane under blue light and reverts to the cytoplasm in the dark. From the membrane-bound (lit) state, elevated temperatures induce dissociation from the membrane, and lower temperatures induce reassociation. B) Representative images showing translocation to the membrane when exposed to blue light in HEK 293T cells. Scale bar represents 15 μm. C) Extended illumination at elevated temperatures (2 hr at 37°C, left) causes subsequent disassociation from the membrane, but reversion to lower temperatures (25°C, right) allows reassociation with the membrane. D) Schematic of Melt. Melt is BcLOV4 with a Q356N mutation, which mimics the lit state of BcLOV4. E) Representative images showing that Melt is cytoplasmic at 37°C and does not translocate to the membrane upon light stimulation, unlike BcLOV4 (E). However, Melt retains temperature sensitivity and translocates to the

membrane upon lowering temperature to 25°C (F). Scale bar = 15 μm. Comparison of optical (G) and thermal (H) responses of wt BcLOV and Melt. See **Figure S1** for details on quantification. Data represent mean +/- 1 SEM of ~100 cells.

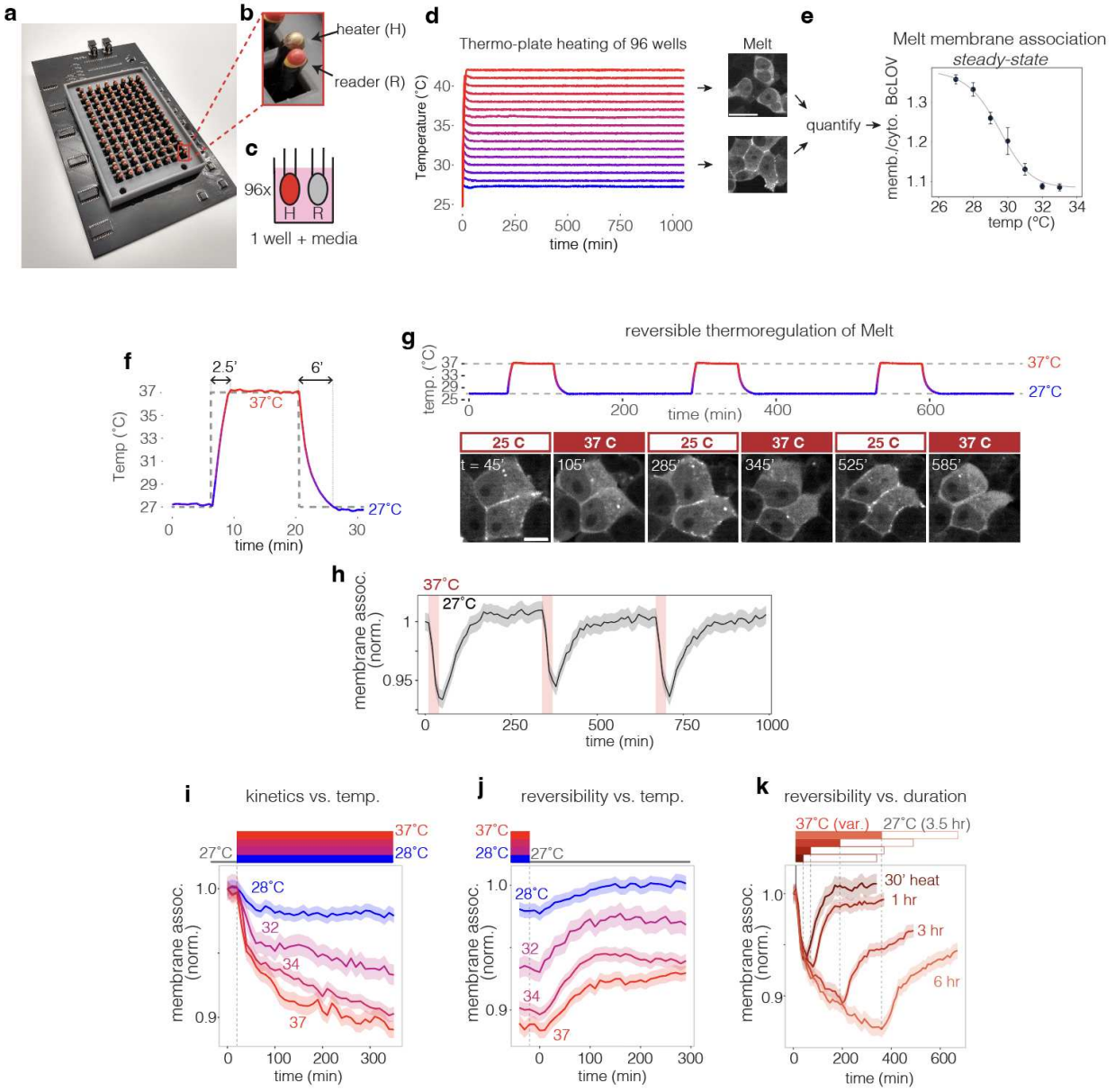

Fig. 2: Characterization of Melt membrane association using the thermoPlate. A) Image of the thermoPlate, a device for thermal control of individual wells in 96-well plate format. B) The thermoPlate consists of 96 pairs of thermistors, which serve as temperature readers (R) and heaters (H). C) Schematic of an H/R pair inserted in the well of a 96 well plate. Simultaneous heating and reading of temperature allows PID feedback-controlled heating. D) Heating of 16 individual wells in a 96-well plate with <1°C resolution over 16 hours. Each trace represents the temperature in a single well as recorded by the (R) thermistor in each well. Scale bar represents 20μm. E) thermoPlate heating of HEK 293T cells stably expressing Melt allowed measurement of steady-state membrane association (14 hr of heating). Data points represent mean +/- 1 SD of three wells, each containing ~200 imaged cells. F) Rapid heating and cooling kinetics enabled by the thermoPlate. Trace shows a single well heated to 37°C for 30 min and subsequent return to 27°C. A 10°C change in setpoint temperature is achieved in ~2.5 and 6

min for heating and cooling, respectively. G) Representative images of live-cell images showing Melt membrane binding over multiple cycles of 1 hr at 37°C followed by 3 hr at 27°C. Scale bar = 10 μm. H) Plot of membrane bound Melt while undergoing cycles of 30 min at 37°C followed by 5 hr at 27°C. Traces represent mean +/- 1 SEM of ~100 cells. I) Kinetics of Melt membrane dissociation when exposed to various temperatures after 24 hr of culture at 27°C. J) Kinetics of Melt membrane reassociation at 27°C after prior exposure to 6 hrs of the indicated temperatures. K) Kinetics of Melt membrane reassociation at 27°C after prior exposure to 37°C for the indicated durations. Each trace in (I-K) represents the mean +/- 1 SEM of ~1000 cells. Data were collected from HEK 293T cells that stably expressed Melt-mCh. For H, I, J, and K membrane binding was normalized to the first time point of each condition.

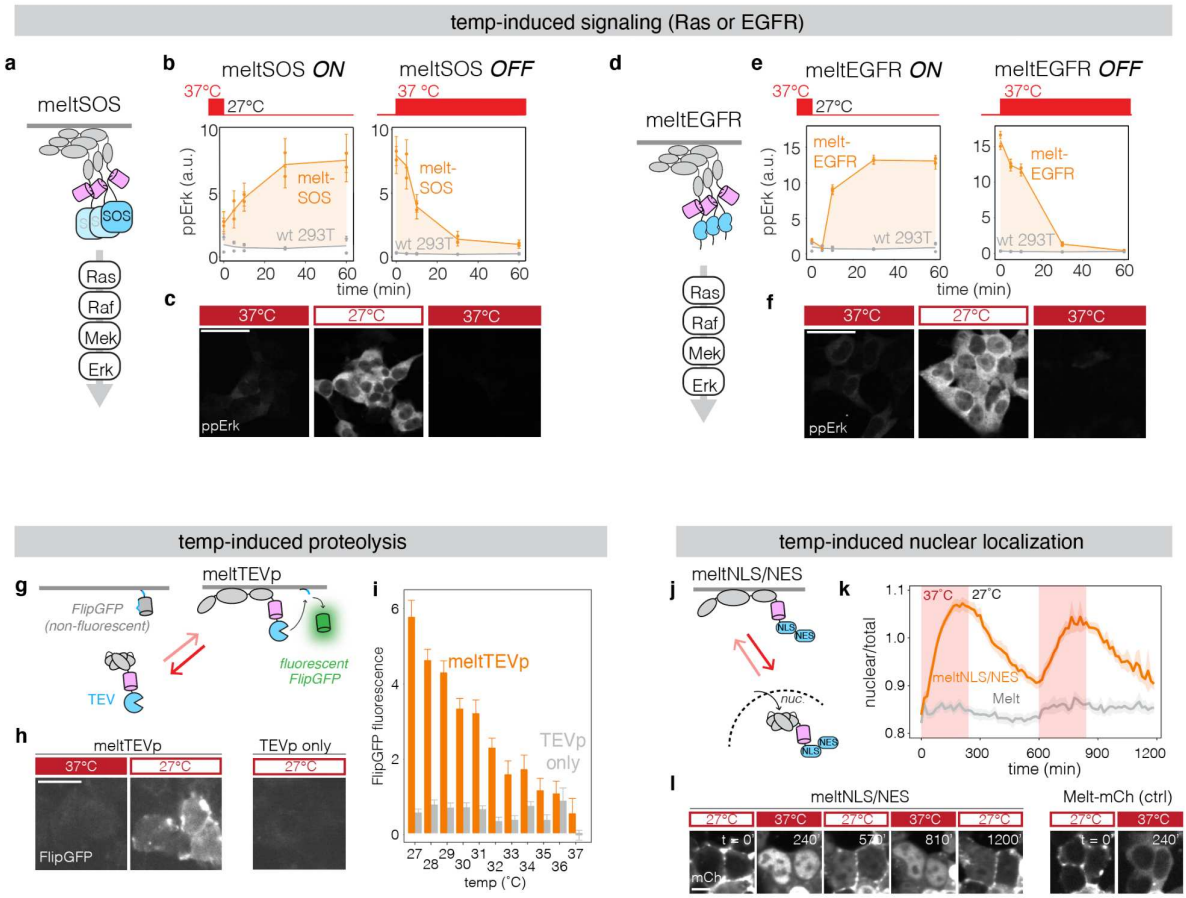

Fig. 3: Thermal control over diverse intracellular processes using Melt. A) Schematic of thermal control of Ras-Erk signaling by membrane recruitment of the SOS2 catalytic domain (meltSOS). B) Thermal activation and inactivation of Ras as assayed by immunofluorescence for activation of the downstream Erk kinase (phospho-Erk, or ppErk). Data points represent the mean +/- 1 SEM of ~500 cells. C) Representative images of ppErk immunofluorescence from meltSOS-expressing cells cultured at the indicated temperatures for 24 hours, 1 hour, and 1 hour respectively. Scale bars represent 40μm. D) Schematic of thermal control of EGFR receptor signaling by membrane recruitment and clustering of the EGFR intracellular domain (meltEGFR). E) Thermal activation and inactivation of EGFR, assayed through immunofluorescence for ppErk. Each data point represents the mean +/- 1 SEM of ~500 cells. F) Representative images of ppErk immunofluorescence from meltEGFR cells cultured at the indicated temperatures for 24 hours, 1 hour, and 1 hour respectively. Scale bars represent 40μm. G) Schematic of thermal control of proteolysis with meltTEVp. At low temperatures, meltTEVp translocates to the membrane where it cleaves a membrane-bound fluorescent reporter of proteolysis (FlipGFP). H) Representative images of FlipGFP fluorescence in cells expressing meltTEVp or TEVp cultured at 37°C or 27°C for 24 hr. Scale bars = 20 μm. I) Quantification of FlipGFP fluorescence in cells expressing either meltTEVp or TEVp cultured at the indicated temperature for 24 hours. Each bar represents the mean +/- 1 SEM of ~1000 cells, normalized between negative and positive controls at each temperature (see **Figure S2** for normalization process). J) Schematic of thermal control of nuclear translocation with meltNLS/NES. K) Quantification of nuclear localization meltNLS/NES and Melt-mCh exposed to

cycles of 37°C and 27°C. Traces represent the mean +/- 1 SEM of ~1000 cells. See **Methods** for details on quantification of nuclear localization. L) Representative images of nuclear localization of meltNLS/NES and Melt-mCh at the temperatures/timepoints found in (K). Scale bar represents 10 μm.

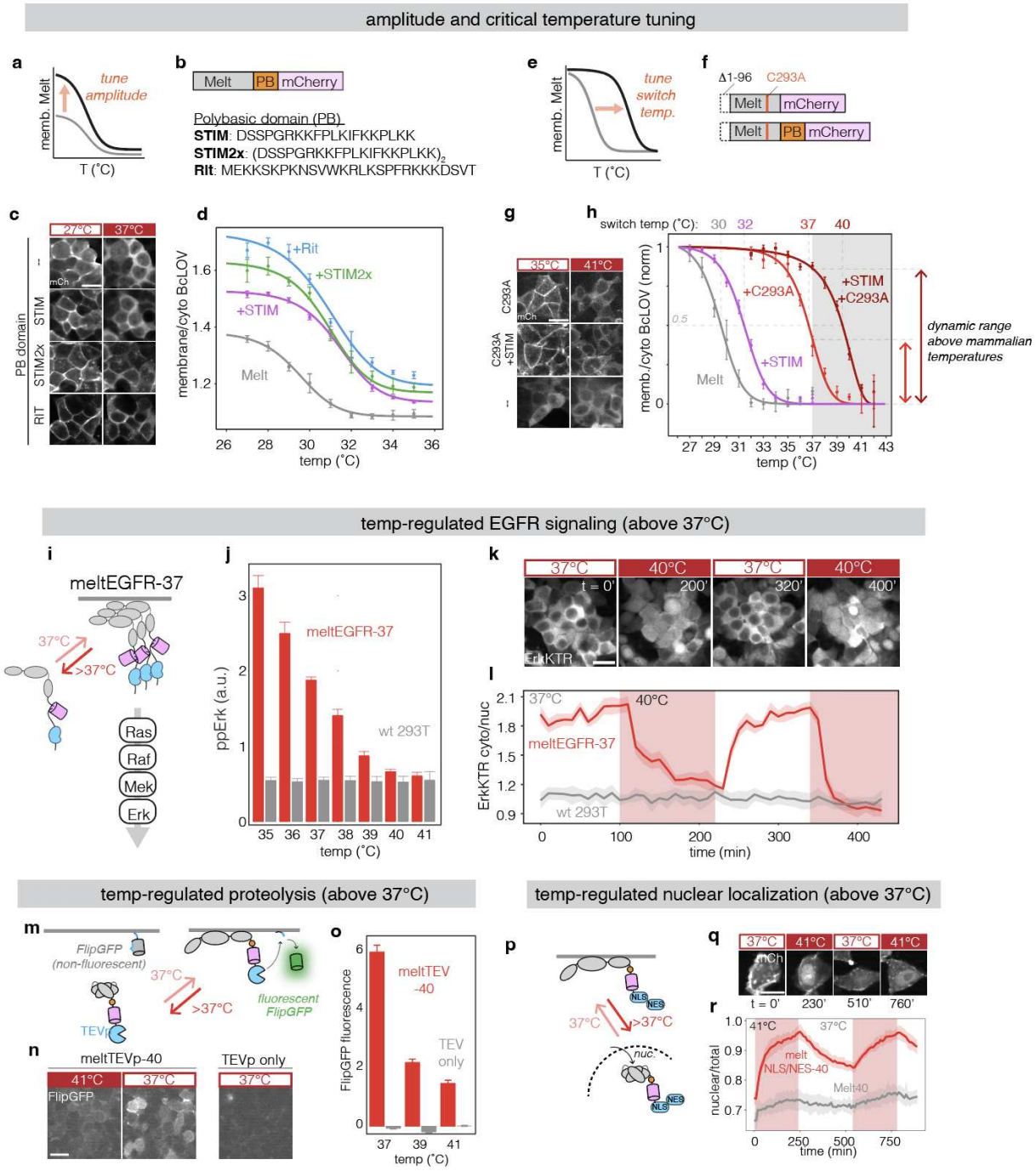

Fig. 4: Tuning of Melt membrane binding and thermal switch-point allows application of Melt-based tools in mammalian temperature ranges. A) Tuning the amplitude of Melt membrane association. B) Polybasic (PB) domains from the STIM or Rit proteins were fused to Melt to test their ability to increase Melt membrane binding strength. C) Representative images showing stronger membrane binding (higher membrane/cyto ratio) of Melt fused to PBs compared to Melt alone. Melt constructs were stably expressed in HEK 293T cells and are shown after 24 hrs of culture at 27°C and after subsequent heating to 37°C for 6 hrs. Scale bar = 20 µm. D) Quantification of steady-state membrane association of Melt-PB fusions after

589 culture at indicated temperatures for 12 hours. Data represent mean +/- 1 SD of three wells with
590 ~200 cells quantified per well. E) Tuning Melt switch-point temperature for use within
591 temperature ranges relevant for mammals, between 37°C and 42°C. F) Schematic of Melt with
592 a C293A mutation with and without STIM PB domain. G) Representative images of membrane
593 localization of Melt, Melt+C293A, or Melt+C293A+STIM fusion at 35°C for 24 hours and
594 subsequent culture at 41°C for 6 hours. Scale bar = 20 μm. H) Quantification of steady-state
595 membrane binding (14 hrs) of Melt variants between 27 and 42°C. Data represent mean +/- 1
596 SD of three wells with ~500 cells quantified per well. Data are normalized between min and max
597 values for each construct. Unnormalized traces can be found in **Figure 4D and Figure S5**. I)
598 Thermal control of EGFR at and above 37°C using Melt-37. J) Immunofluorescence
599 quantification of pathway activation in HEK 293T cells stably expressing meltEGFR-37. Cells
600 were incubated at indicated temperatures for 75 min before fixation. Bars represent mean +/- 1
601 SD of three wells with ~1000 cells quantified per well. K) meltEGFR-37 activation visualized
602 through the live-cell ErkKTR reporter. Nuclear depletion of ErkKTR indicates Erk activation
603 while nuclear enrichment indicates Erk inactivation. Scale bar represents 10 μm. L)
604 Quantification of ErkKTR activity (cyto/nuclear ratio) in HEK 293T cells expressing meltEGFR-
605 37 or wt cells. Traces represent mean +/- 1 SD of ~15 cells per condition. M) Control of
606 proteolysis at mammalian temperatures with meltTEVp-40. N) Representative images of
607 FlipGFP signal in cells expressing meltTEVp-40 or TEVp after incubation at the indicated
608 temperatures for 24 hours. Scale bar represents 10 μm. O) Quantification of FlipGFP signal in
609 fixed cells expressing meltTEVp-40 or TEVp cultured at the indicated temperatures for 24 hours.
610 Each bar represents the mean +/- 1 SEM of ~1000 cells. Y-axis represents mean fluorescence
611 subtracted by the signal of TEVp-negative cells. P) Control of nuclear translocation at
612 mammalian temperatures with meltNLS/NES-40. Q) Representative images of nuclear
613 translocation. Scale bar represents 20 μm. R) Quantification of nuclear localization of
614 meltNLS/NES-40 or Melt-40-mCh after exposure to cycles of 37°C and 41°C (red) in HEK 293T
615 cells. Traces represent the mean +/- 1 SEM of ~1000 cells.

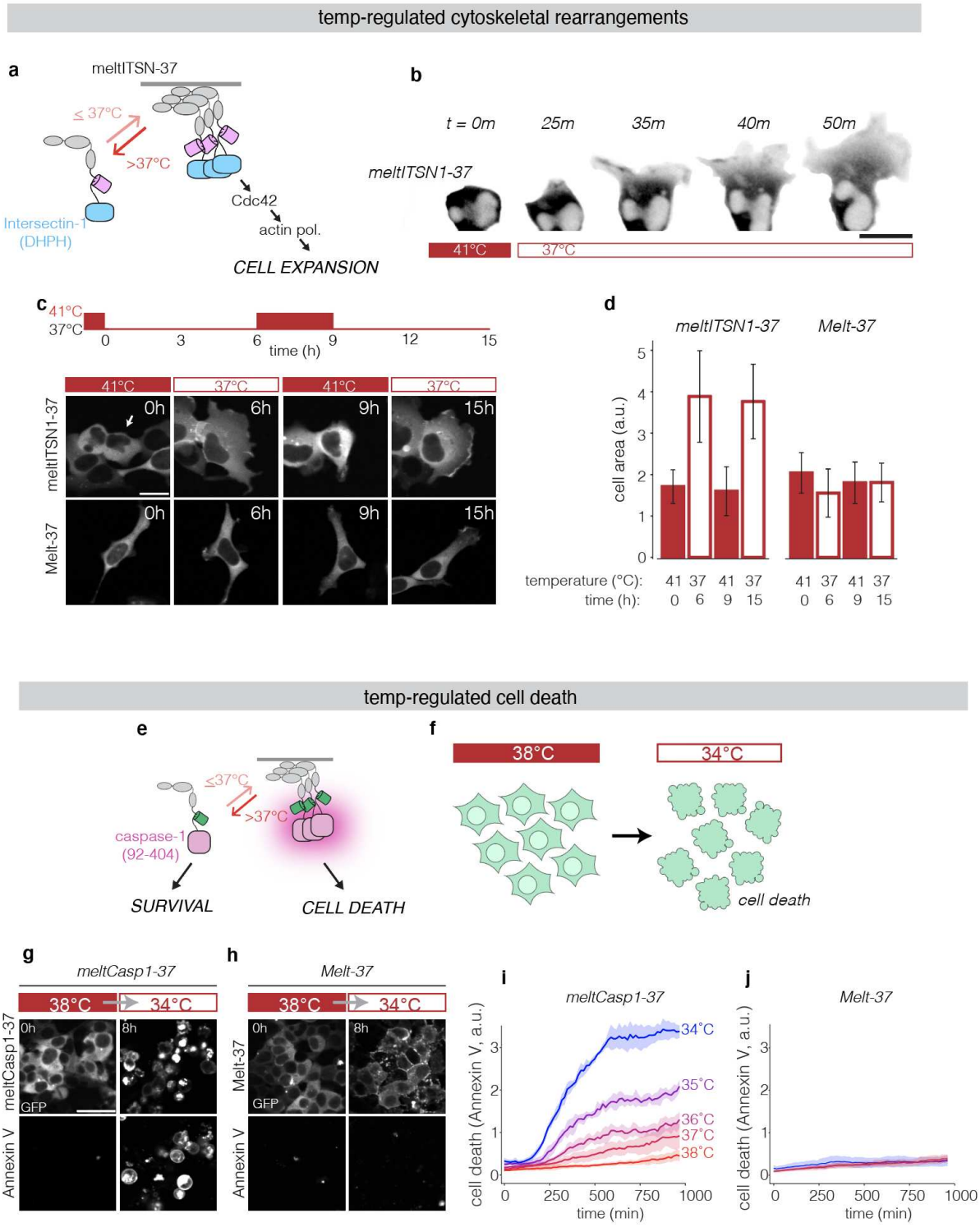

Fig. 5: Thermal regulation of cell fate using Melt. A) Control of Cdc42 activity and cell shape through recruitment of the DHPH domain of ITSN1 to the membrane. B) Representative images of cell shape changes in response to temperature control in a HEK 293T cell transiently expressing meltITSN1-37. Upon reduction of temperature from 41°C to 37°C, cells show rapid formation of membrane extensions and dramatic increase in size. Scale bars = 20 μm. C) Cell

shape changes are reversible and repeatable over several hours of stimulation. Representative images of HEK 293T cells transiently transfected with meltITSN1-37, cultured at 41°C and exposed to multiple rounds of heating and cooling at the times and temperatures indicated. Scale bars = 20μm. D) Quantification of cell area of cells expressing either meltITSN1-37 or Melt-37 after repeated cooling and heating. Bars represent the average cell size of 15 cells +/- 1 SD. E) Thermal control of cell death through regulation of caspase-1 clustering (meltCasp1-37). F) meltCasp1-37 induces cell death upon lowering temperature below 37°C. G) Representative images of cells expressing meltCasp1-37 (G) or Melt-37 (H) before and after exposure to 34°C for 8 hours after culture at 38°C for 24 hours. Bottom panels of (G,H) show AnnexinV-647 staining, which indicates cell death. Scale bars = 40 μm. I) Quantification of AnnexinV intensity in meltCasp1-37 and Melt-37 cells over time at the indicated temperature after prior culture at 38°C for 24 hours. Plots represent the mean +/- SEM of per-image AnnexinV fluorescence divided by total GFP fluorescence (to account for cell density) across 4 images. See **Methods** for quantification details. All images/data in this figure were collected from transient expression of Melt constructs in HEK 293T cells.

METHODS

Cell Culture

Lenti-X HEK 293T cells were maintained in 10% fetal bovine serum (FBS) and 1% penicillin/streptomycin (P/S) in DMEM. (Lenti-X HEK 293T: Takarabio 632180). Cell lines were not verified after purchase. Cells were not cultured in proximity to commonly misidentified cell lines.

Plasmid design and assembly

Constructs for stable transduction and transient transfection were cloned into the pHR lentiviral backbone with a CMV promoter driving the gene of interest. Melt mutations were introduced to WT BcLOV4 (Provided by Brian Chow) (Addgene Plasmid #114595) via whole backbone PCR using primers containing the target mutation. Mutations were introduced using the same primers on BcLOV4-ITSN1 (Provided by Brian Chow) (Addgene #174509) to generate meltITSN1-37. Melt-PB fusions were generated via whole backbone PCR using primers containing PB coding sequences (**Figure 2B**). PCR products were circularized via ligation (New England Biolabs). For Melt-effector fusions, the pHR backbone was linearized using MluI and NotI restriction sites. Melt, TEVp (Addgene Plasmid #8827), EGFR (sourced from Opto-hEGFR, which was a kind gift from Dr. Harold Janovjak), SOS [18], and Caspase-1 (Provided by Peter Broz) [39] were generated via PCR and inserted into the pHR backbone via HiFi cloning mix (New England Biolabs). All Melt37/40-Effector fusions were generated by amplifying Melt37/40 with primers that amplified the region downstream of a.a.96 such that the final Melt variants contained a a.a.1-96 deletion. NLS/NES insertions were generated via backbone PCRs with NLS/NES sequences (**Figure S3**) incorporated into the primers. To construct FlipGFP-BFP-CAAX, the two fragments of FlipGFP B1-9 and B10-E5-B11-TEVcs-K5 were amplified from Addgene Plasmid #124429 via PCR. tagBFP [18] was amplified using primers containing a CAAX membrane binding sequence. These fragments were assembled in the linearized PHR backbone via HiFi cloning mix in the order B1-9-P2A-B10-E5-B11-TEVcs-K5-tagBFP-CAAX. In order to reduce affinity of TEVp for the TEV cut site (cs) and lower basal proteolysis, the canonical cut site ENLYFQS was mutated to ENLYFQL [45] via whole backbone PCR using primers harboring the mutation. GFP-CAAX was generated via PCR of eGFP using primers containing the CAAX sequence and cloned into the linearized viral backbone using HiFi cloning mix.

Plasmid transfection.

HEK 293T cells were transfected using the calcium phosphate method, as follows: Per 1 mL of media of the cell culture to be transfected, 50 µL of 2x HeBS[28,29] buffer, 1 µg of each DNA construct, and H_2O up to 94 µL was mixed. 6 µL of 2.5mM $CaCl_2$ was added after mixing of initial components, incubated for 1:45 minutes at room temperature, and added directly to cell culture.

Lentiviral packaging and cell line generation

Lentivirus was packaged by cotransfecting the pHR transfer vector, pCMV-dR8.91 (Addgene, catalog number 12263), and pMD2.G (Addgene, catalog number 12259) into Lenti-X HEK293T. Briefly, cells were seeded one day prior to transfection at a concentration of 350,000 cells/mL in

a 6-well plate. Plasmids were transfected using the calcium phosphate method. Media was removed one day post-transfection and replaced with fresh media. Two days post-transfection, media containing virus was collected and centrifuged at 800 x g for 3 minutes. The supernatant was passed through a 0.45 µm filter. 500 µL of filtered virus solution was added to 700,000 HEK293T cells seeded in a 6-well plate. Cells were expanded over multiple passages, and successfully transduced cells were enriched through fluorescence activated cell sorting (Aria Fusion).

Preparation of cells for plate-based experiments

All experiments were carried out in Cellvis 96 well plates (#P96-1.5P). Briefly, wells were coated with 50uL of MilliporeSigma™ Chemicon™ Human Plasma Fibronectin Purified Protein fibronectin solution diluted 100x in PBS and were incubated at 37 °C for 30 min. HEK 293T cells were seeded in wells at a density of 35,000 cells/well in 100 µL and were spun down at 20 x g for 1 minute. In experiments requiring starvation (for all experiments involving SOS and EGFR constructs), after 24 hr, cells were starved by performing 7 80% washes with starvation media (DMEM + 1% P/S). Experiments were performed after 3 hr of starvation.

Fixing and Immunofluorescence staining

Immediately following the completion of a temperature stimulation protocol, 16% paraformaldehyde (PFA) was added to each well to a final concentration of 4%, and cells were incubated in PFA for 10 min. For immunofluorescence staining, cells were then permeabilized with 100 µL phosphate buffered saline (PBS) + 0.1% Triton-X for 10 min. Cells were then further permeabilized with ice cold methanol for 10 min. After permeabilization, cells were blocked with 1% BSA at room temperature for 30 min. Primary antibody was diluted in PBS + 1% BSA according to the manufacturer's recommendation for immunofluorescence (phospho-p44/42 MAPK (Erk1/2) (Thr202/Tyr204), Cell Signaling #4370, 1:400 dilution; phospho-Rb (Ser807/811) Cell Signaling #9308, 1:800 dilution; Anti-Human G3BP1, BD Biosciences #611126, 1:500 dilution). Wells were incubated with 50 µL of antibody dilution for 2 hr at room temperature (RT), after which primary antibody was removed and samples underwent five washes in PBS + 0.1% TWEEN-20 (PBS-T). Cells were then incubated with secondary antibody (Jackson Immunoresearch Alexa Fluor® 488 AffiniPure Goat Anti-Rabbit IgG (H+L) or Invitrogen Goat anti-Mouse IgG (H+L) Cross-Adsorbed Secondary Antibody, DyLight™ 650) and DAPI (ThermoFisher, #D1306, 300 nM) in PBS-T + 0.1% BSA for 1 hour at RT. Secondary antibody was removed, samples underwent 5 washes with PBS-T. Samples were imaged in PBS-T.

Imaging

Live-cell imaging. Live-cell imaging was performed using a Nikon Ti2-E microscope equipped with a Yokagawa CSU-W1 spinning disk, 405/488/561/640 nm laser lines, an sCMOS camera (Photometrics), a motorized stage, and an environmental chamber (Okolabs). HEK 293Ts

expressing the construct of interest were imaged with a 20X or 40X objective at variable temperatures and 5% CO_2. Optogenetic BcLOV4 was stimulated using a 488nm laser.

High content fixed-cell imaging. Fixed samples were imaged using a Nikon Ti2E epifluorescence microscope equipped with DAPI/FITC/Texas Red/Cy5 filter cubes, a SOLA SEII 365 LED light source, and motorized stage. High content imaging was performed using the Nikon Elements AR software. Image focus was ensured using image-based focusing in the DAPI channel.

Image processing and analysis

Immunofluorescence quantification. Images were processed using Cell Profiler. Cells were segmented using the DAPI channel, and cytoplasm was identified using a 5 pixel ring around the nucleus. Nuclear and cytoplasmic fluorescence values were then exported and analyzed using R (https://cran.r-project.org/) and R-Studio (https://rstudio.com/). Data was processed and visualized using the tidyR [46] and ggplot2 [47] packages.

Membrane recruitment. Membrane localization was quantified using the MorphoLibJ plugin for ImageJ [48]. Briefly, MorphoLibJ was used to segment single cells based on a constitutively membrane bound GFP-CAAX marker. The resulting segmentation was imported into Cell Profiler and was used to quantify the amount of mCherry (fused to the protein of interest) localized to the membrane as well as total mCh per cell (**Figure S1**). Total mCh and membrane-localized mCh intensity was recorded and further processed in R. Bleaching was corrected by dividing the membrane intensity of mCh by total cell mCh.

FlipGFP Quantification. Cells expressing membrane bound FlipGFP-CAAX and the indicated TEVp construct were grown at the indicated temperature and fixed in 4% PFA after 24 hours. FlipGFP was tethered to the membrane via a Blue Fluorescent Protein (TagBFP)-CAAX fusion. BFP-CAAX remained tethered to the membrane before and after proteolysis and thus could be used as a membrane marker. This marker was used to segment single cells using the same workflow used for membrane recruitment quantification. Single cell GFP levels were quantified using Cell Profiler and used as an indicator of relative levels of proteolysis.

Nuclear Localization. To quantify nuclear localization of a protein of interest, cells expressing a GFP-CAAX membrane marker (see above) were transfected with an H2B-iRFP nuclear marker. The above workflow was used to segment individual cells based on the membrane marker. This segmentation was imported to CellProfiler, which was also used to segment nuclei based on iRFP imaging. Each nucleus was then assigned to a parent cell. Nuclei were assigned to a cell if >90% of the nucleus object was contained by the cell object. Membrane segmented cells that contained no nuclei objects or nuclei that were not within a parent cell were eliminated from quantification. Finally, nuclear to total cell mCherry (used as a marker fused to the protein of interest) was calculated and recorded for each cell.

Annexin Staining and Quantification. Annexin V-647 (Invitrogen A23204) was added to 100 µL of cell culture at a 1:100 final dilution. A final concentration of 1 mM $CaCl_2$ was also added to each well to allow Annexin V cell labeling. Cell media was removed and replaced with Annexin

V media 30 min prior to imaging. To quantify Annexin V, images of cells expressing meltCasp1-37 or Melt-37 both with a GFP fusion were used to create GFP masks using CellProfiler's threshold function. Annexin images were masked for GFP positive pixels. The total masked Annexin image intensity was recorded and normalized by the number of GFP positive pixels (cell area per image) in each image.

Cell Area Quantification. Cell area was measured semi-manually. Images of cells expressing meltITSN1-37 and Melt-37 were imaged and resulting images were thresholded in ImageJ such that cell positive pixels were set to 1 and background pixels were set to 0. Cells were manually chosen for quantification and regions containing the cell of interest were drawn by hand. Measuring integrated pixel intensity of these regions gave rise to the number of cell positive pixels in that region which was used as a metric of total cell area. For further explanation, see **Figure S9**.

Curve fitting

Data points for Melt variant equilibrium membrane binding at various temperatures were fit to the Hill Equation (Eq.1). MATLAB was used to minimize the error between the sigmoid function and each data point. The characteristic function used for fitting was:

$$F(x) = A * x^B/(C^B + x^B) \quad \text{(Eq. 1)}$$

A, B, and C were used as the adjusted parameters. These curves are displayed in **Figure 2E, 4D, and 4H** with datapoints overlaid. The associated code can be found in this manuscript's code repository (https://rb.gy/1k7tc).

Supplemental Figures

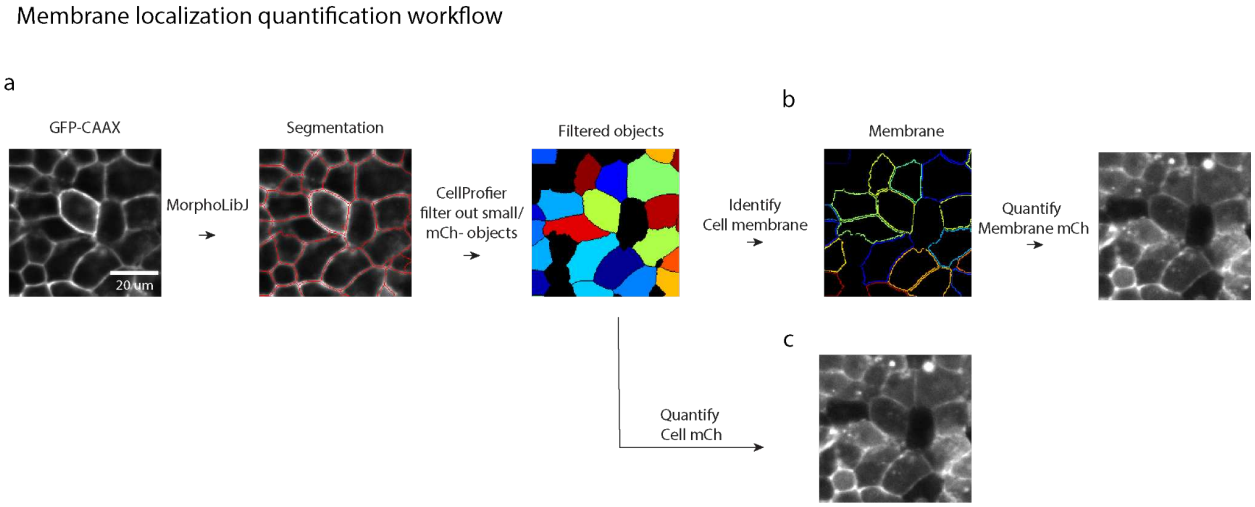

Figure S1. Schematic of workflow for quantification of membrane association. Experiments were performed in cells stably expressing a GFP-CAAX membrane marker. Image analysis was performed using the MorphoLibJ plugin for ImageJ to enable segmentation of cell borders. The resulting segmentation was imported into CellProfiler which was then used to filter out objects below a size threshold, eliminating cell fragments, and cells not expressing mCherry (used as a fluorescent tag for all Melt constructs quantified). From there, segmented cells could be used to quantify total mCh levels in each cell. Additionally, a 1 pixel radius at the edge of the object was assigned as the cell membrane and was used to quantify membrane levels of mCh.

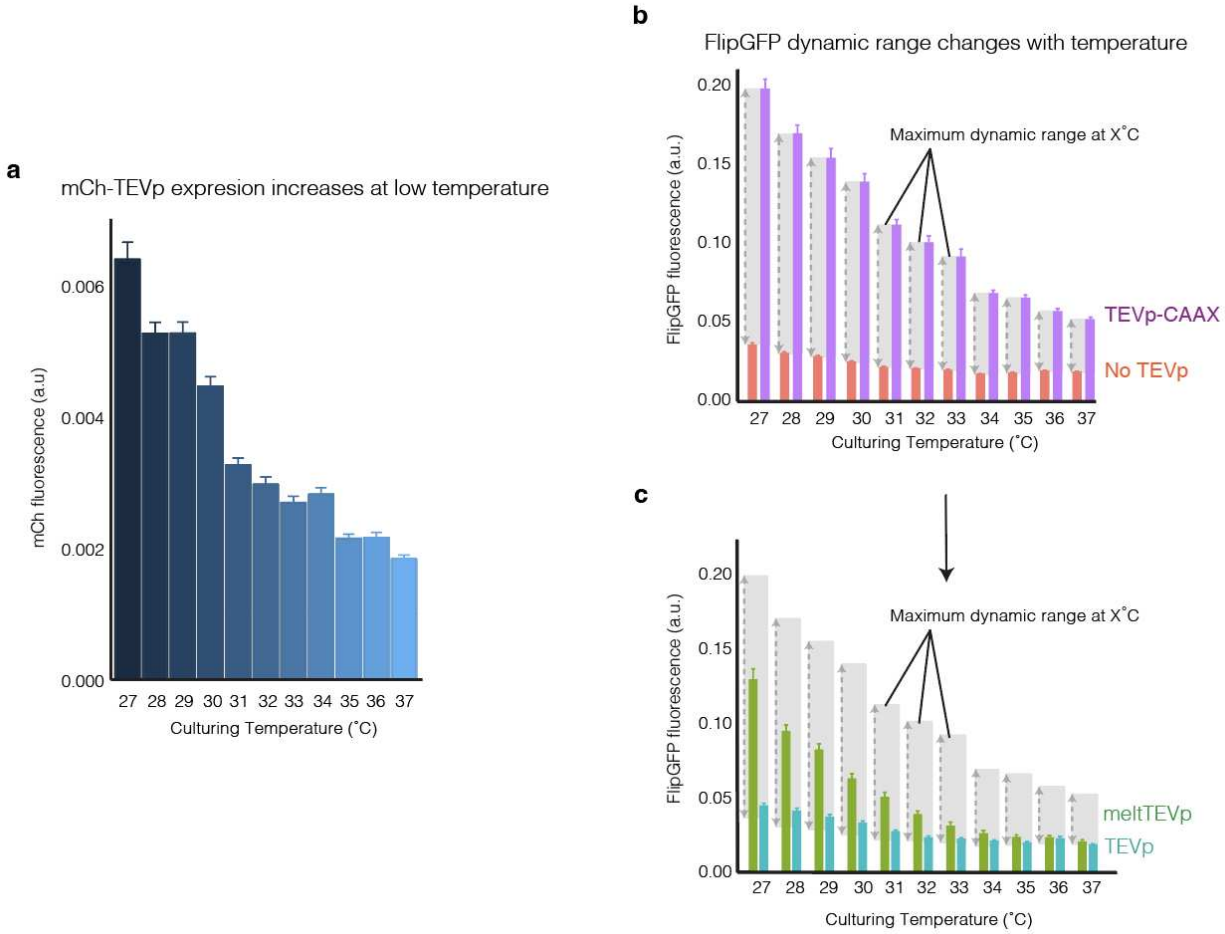

Figure S2. Normalization of meltTEVp proteolysis to account for temperature-dependent changes in protein expression. A) Total protein expression is elevated at low temperatures as demonstrated by mCh-TEVp expression. Cells were cultured at the indicated temperature for 24 hours. B) To account for changes in FlipGFP signals caused by temperature dependent expression differences, negative control (no TEVp) and positive control (constitutively membrane bound TEVp-CAAX) cells were used to establish minimal and maximal FlipGFP signals at each temperature. C) Minimal and maximal cutting ranges at each temperature were used to normalize meltTEVp and TEVp proteolysis to the ranges established in (B) (subtracting minimum signal and dividing by maximum). This normalization was performed to account for changes in protein expression levels that could account for increases in proteolysis at low temperatures. Each bar in all plots represents the mean +/- 1 SEM of ~1000 cells.

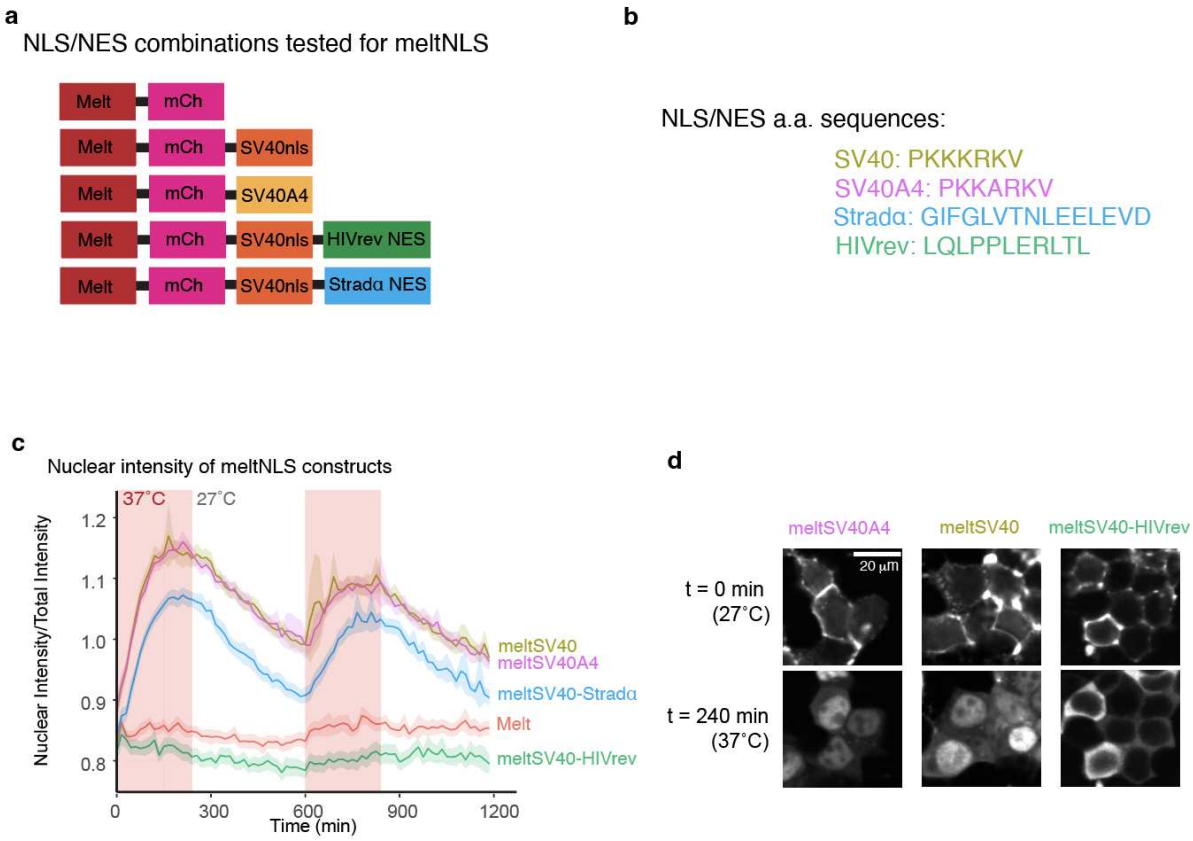

Figure S3. **Different NLS/NES combinations achieve varying levels of nuclear shuttling.** A) Diagram of all meltNLS/NES fusions tested in order to achieve the largest dynamic range of nuclear shuttling between 27°C and 37°C. B) Amino acid sequence of NLS and NES used in meltNLS/NES fusions. C) Quantification of nuclear Melt signal using the five constructs shown in A exposed to repeated cycles of heating and cooling. Traces represent the mean of ~1000 cells +/- SEM. D) Representative images of meltNLS/NES combinations before and after heating to 37°C and cooling to 27°C.

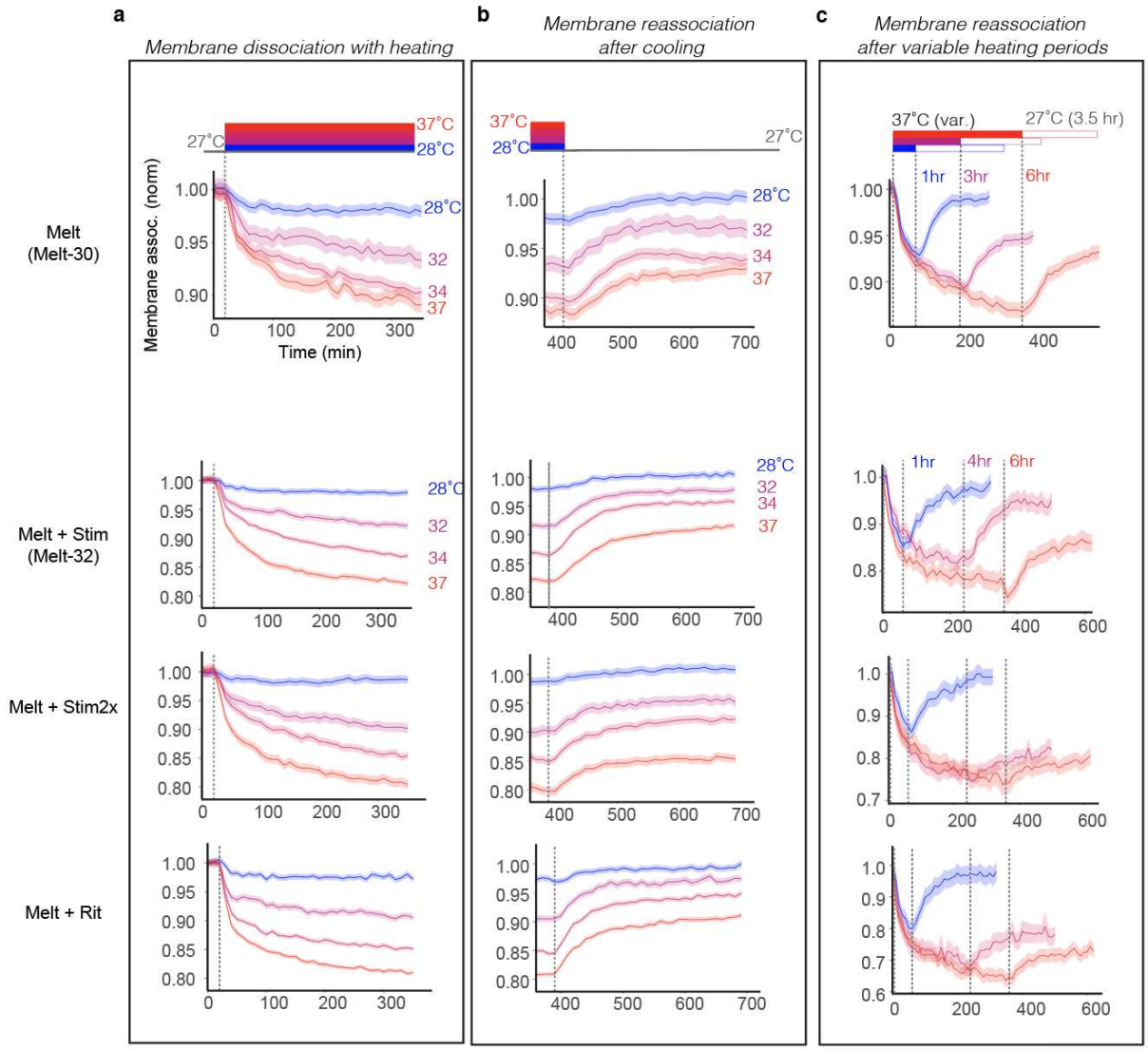

Figure S4. **Kinetics of membrane dissociation and reassociation of Melt-PB fusions.** A) Quantification of membrane dissociation at the indicated temperature after prior culture at 27°C for 24 hours. Dashed lines indicate the time at which the temperature was raised to the indicated temperature. B) Quantification of membrane recruitment of the indicated construct cultured at 27°C after previous culture at the indicated temperature for the preceding 6 hours. Traces represent the kinetics of membrane reassociation and are continuations of traces found in (A). Dashed lines indicate the time at which the temperature was lowered from the indicated temperature. C) Quantification of membrane recruitment of the indicated construct during culture at 37°C after culture at 27°C for 24 hours. Dashed lines indicate the time at which cells were returned to 27°C to identify the effect of different periods of heating on membrane reassociation kinetics. All traces represent the mean of ~1000 cells +/- SEM. Membrane binding for all plots was normalized to the first time point of each condition.

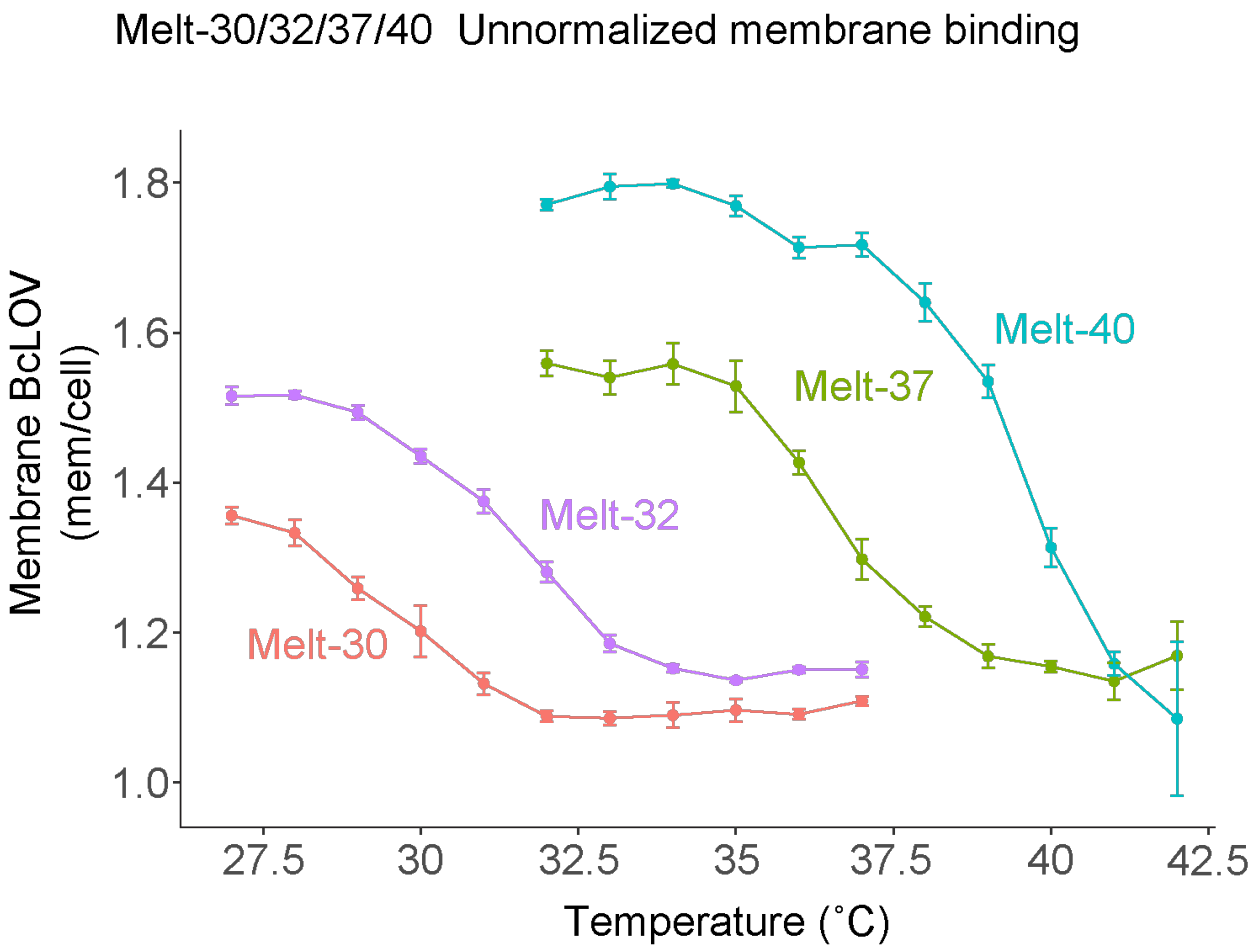

Figure S5. **Relative membrane binding of Melt variants.** Unnormalized plots of data shown in **Figure 4H**, showing relative membrane binding strength of Melt-30/32/37/40 at the indicated temperatures. Each point represents the average of three wells +/- SD with ~500 cells quantified in each well.

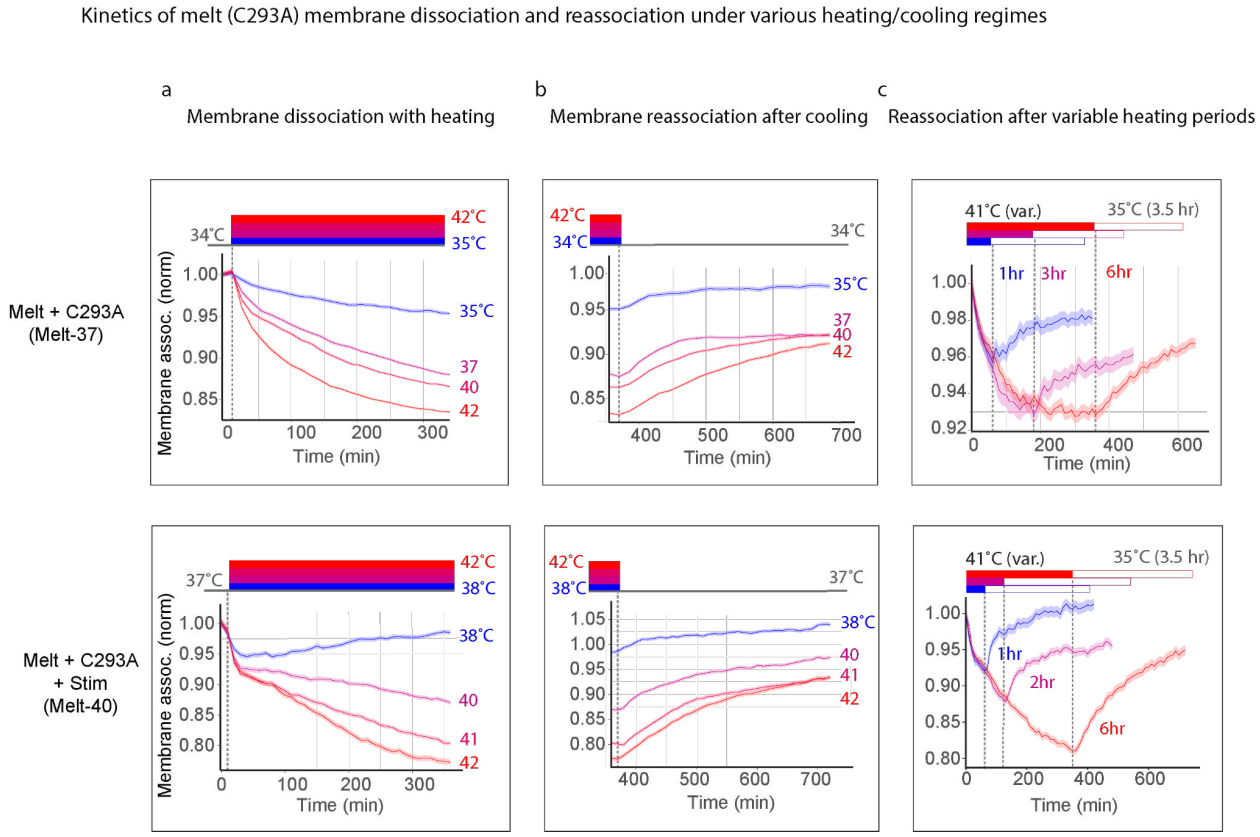

Figure S6. **Kinetics of membrane dissociation and reassociation of Melt variants.** A) Quantification of membrane recruitment of the indicated construct cultured at the indicated temperatures. Traces represent the kinetics of membrane dissociation after prior culture at either 34°C (C293A) or 37°C (C293A+Stim) for 24 hours. Dashed lines indicate the time at which the temperature was raised to the indicated temperature. B) Quantification of membrane recruitment of the indicated construct cultured at 34°C (C293A) or 37°C (C293A+Stim) after prior culture at the indicated temperature for the preceding 6 hours. Traces represent the kinetics of membrane reassociation and are continuations of traces found in (A). Dashed lines indicate the time at which the temperature was lowered from the indicated temperature. C) Quantification of membrane recruitment of the indicated construct during culture at 41°C after prior culture at 35°C for 24 hours. Dashed lines indicate the time at which cells were returned to 35°C to identify the effect of different periods of heating on membrane reassociation kinetics. All traces represent the mean of ~1000 cells +/- SEM. Membrane binding for all plots was normalized to the first time point of each condition.

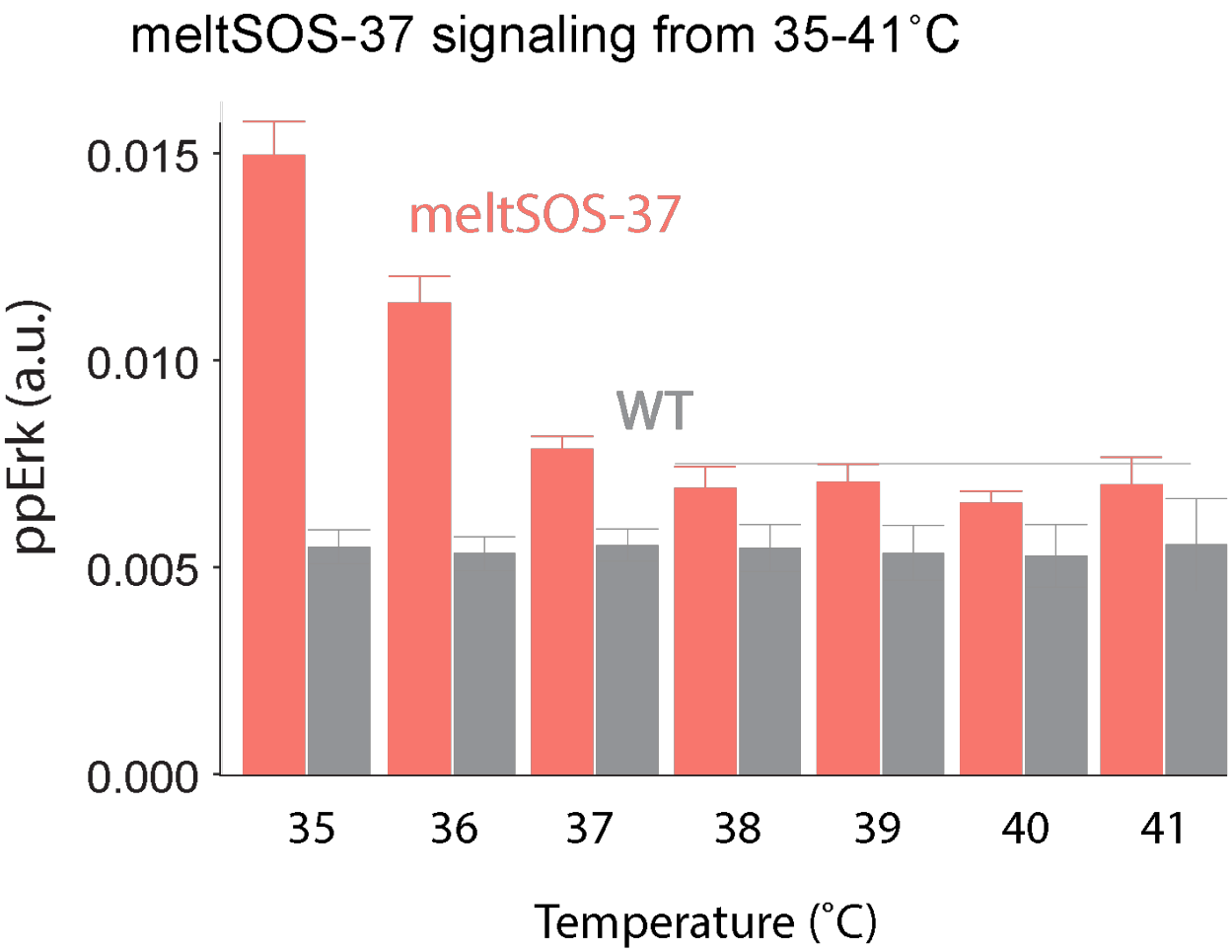

Figure S7. **Thermal activation of meltSOS-37**. meltSOS-37 achieves signaling activation at temperatures < 37°C. Plot showing quantification of pathway activation (single-cell immunofluorescence for ppErk) in cells expressing meltSOS-37 exposed to the indicated temperatures for 75 min. Data points represent the mean of 2 wells +/- SD with ~1000 cells quantified per well.

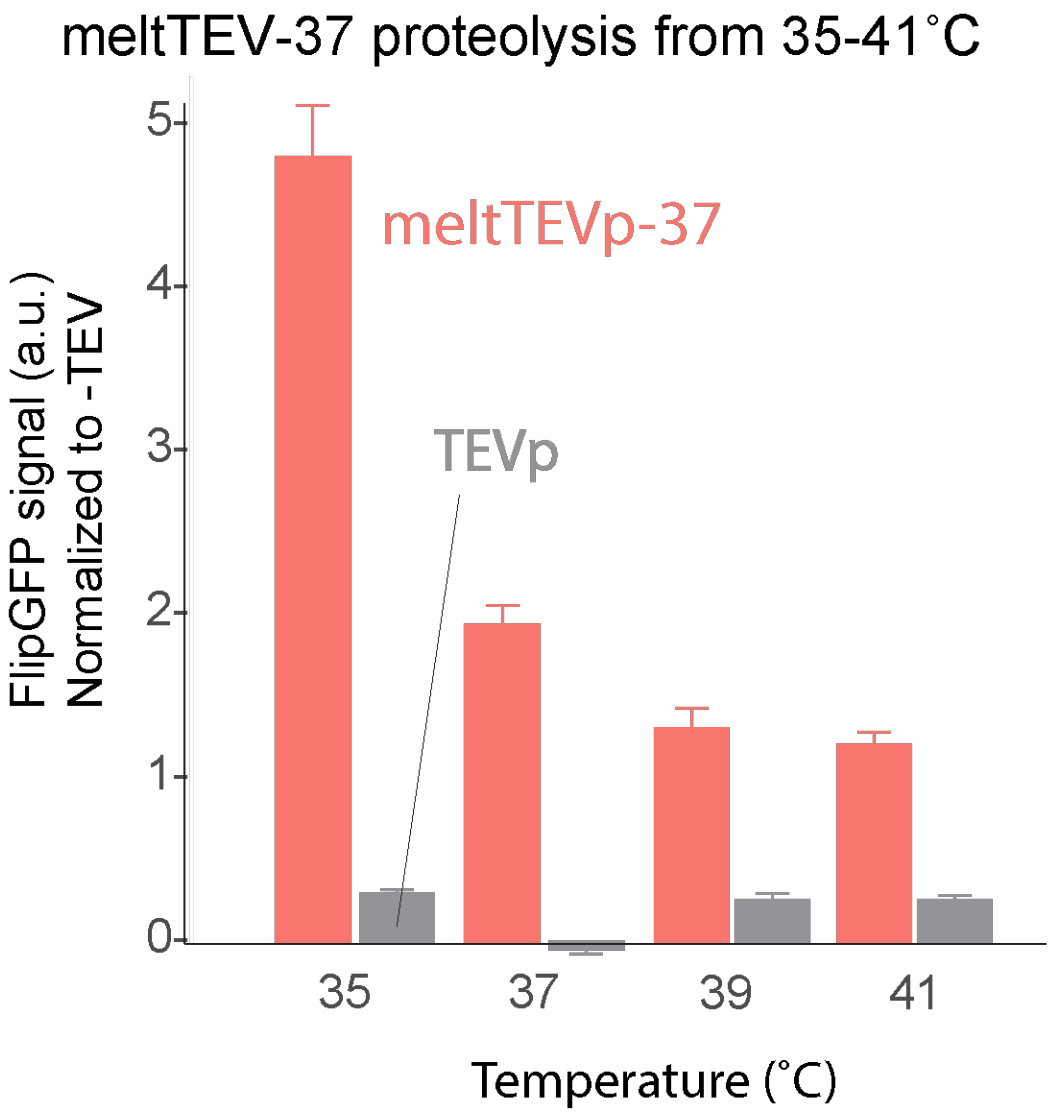

Figure S8. **Thermal activation of meltTEVp-37.** meltTEVp-37 achieves proteolysis at temperatures <37°C. Plot showing FlipGFP fluorescence in cells expressing meltTEVp exposed to the indicated temperatures. Data points represent the mean ~1000 cells +/- SEM. See **Methods** for FlipGFP quantification workflow.

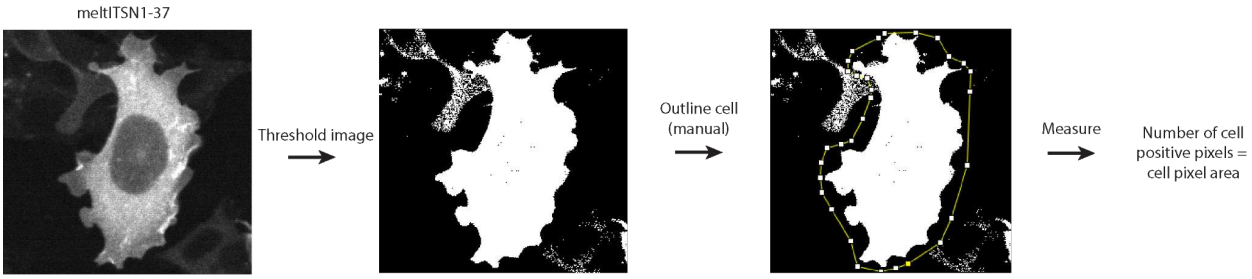

Figure S9. Quantification of cell area to assess effects of meltITSN1-37. A cell expressing meltITSN1-37 was imaged and subsequently thresholded in ImageJ such that cell positive pixels were set to 1 and background pixels were set to 0. A region of interest containing the cell of interest was drawn by hand. Summing the total number of positive pixels in the cell region was therefore used as a metric of total cell area.

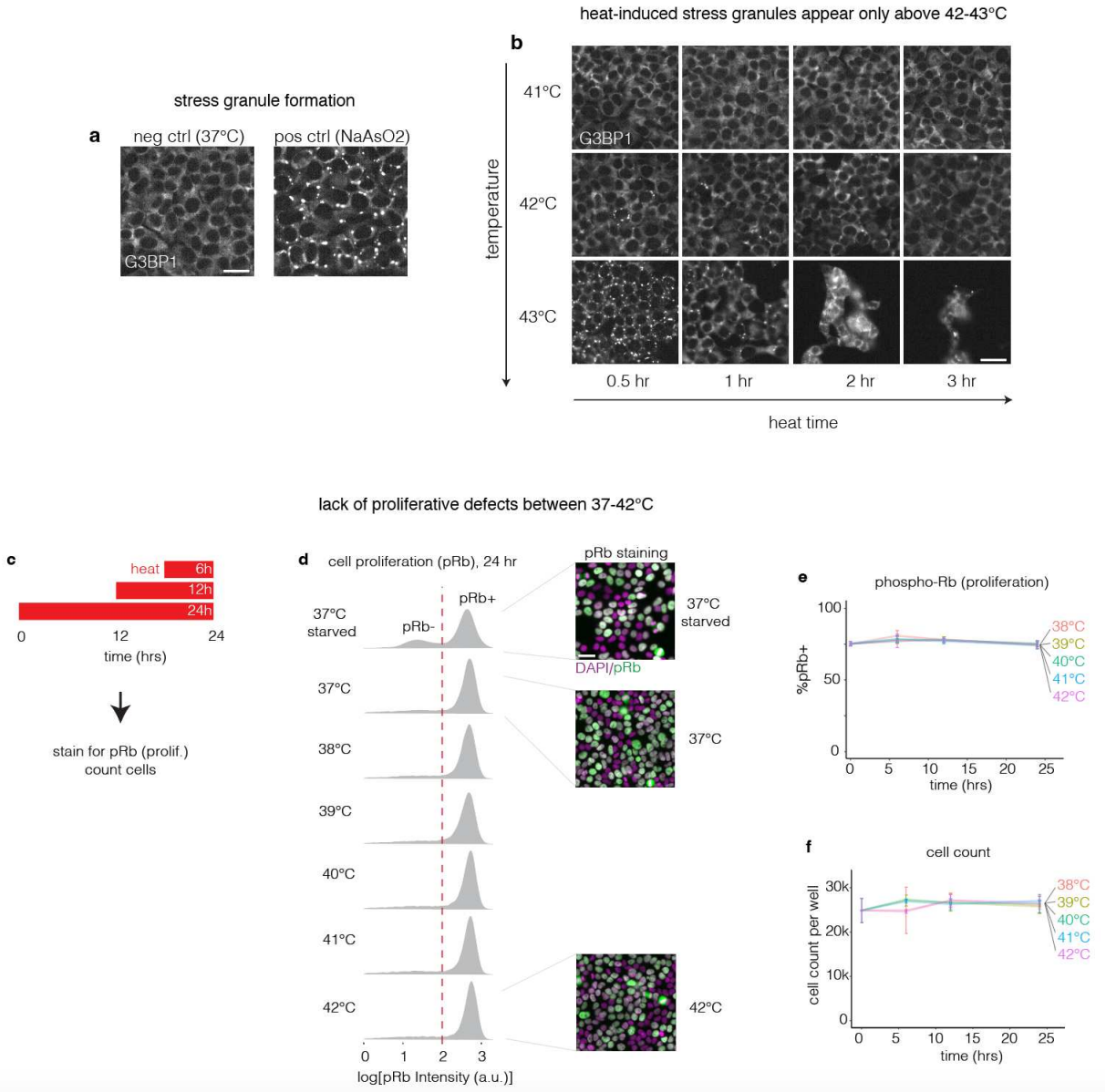

Figure S10. Lack of thermal stress observed below 42°C. To examine whether the temperature changes required for Melt-37/40 activation would also apply thermal stress to mammalian cells, we measured stress granule (SG) formation as well as changes in proliferation in response to thermal stimuli used throughout the manuscript. A) SGs were visualized by immunofluorescence for G3BP1. No SGs were seen in HEK293T cells in normal growth conditions, while bright SG puncta were seen in cells treated with 100 μM sodium arsenite for 3 hours prior to fixation (positive control). B) SGs were visualized in HEK293Ts that were exposed to various durations and intensities of heating. No SGs were observed in cells heated to $\leq$ 41°C, and only a few cells showed SGs when heated to 42°C. By contrast, heating to 43°C induced SGs in nearly all cells within 30 min, followed by detachment of cells at later time points. C) To examine integration of potential heat stress over longer time periods, we measured cell proliferation. D) Staining for phospho-Rb (pRb) indicates whether a cell is in G1 (pRb-) or in later stages of the cell cycle (pRb+). Red line in density plots separates the two populations. HEK293T cells starved for 24 hr (top plot) show a larger fraction of cells in G1 compared to cells kept in full medium (second from top). Cells cultured in full medium for 24 hr at temperatures between 38-

941 42°C show the same fraction of pRb+ cells as cells cultured at 37°C, indicating no stress-induced
942 impairment of proliferation. E) Quantification of pRb+ cells after the indicated times and
943 temperatures of heating. Each data point represents the mean +/- SD of three wells. F)
944 Quantification of total cell counts from experiment in (D,E). The lack of difference in cell counts at
945 different temperatures demonstrates a lack of changes in proliferation or cell death due to heat
946 stimulation at or below 42°C. Each point represents the mean and range of wells. All scale bars
947 in this figure represent 30 μm.
948

Supplementary Movie Captions:

Supplementary Movie 1. Reversible membrane binding of Melt using temperature changes. HEK 293T cells stably expressing Melt were exposed to 1 hour of heating followed by 4 hours of cooling (37° and 27°C respectively) in order to capture dynamic changes in membrane binding at each temperature. Time is hh:mm. Scale bar = 40 μm.

Supplementary Movie 2. Temperature-controlled nucleocytoplasmic shuttling of meltNLS/NES. HEK 293T cells transiently expressing meltNLS/NES were exposed to repeated rounds of 37° and 27°C to observe dynamic changes in nuclear shuttling. Time is hh:mm. Scale bar = 15 μm.

Supplementary Movie 3. Thermal control of Erk activity in mammalian temperature ranges using meltEGFR-37. HEK 293T cells stably expressing meltEGFR-37 were exposed to repeated rounds of 37° and 40°C. Video shows the ErkKTR reporter, which indicates Erk activation through changes in the ratio of cytoplasmic to nuclear fluorescence. Nuclear enrichment of the reporter upon heating indicates reduction of Ras-Erk signaling, while nuclear depletion upon cooling indicates pathway activation. Stills from this movie were used to generate the images found in **Figure 4K**. Time is hh:mm. Scale bar = 10 μm.

Supplementary Movie 4. Temperature-controlled nucleocytoplasmic shuttling of meltNLS/NES-40 in mammalian temperature ranges. HEK 293T cells transiently expressing meltNLS/NES-40 were exposed to repeated rounds of 41° and 37°C in order to capture dynamic changes in nuclear shuttling. Time is hh:mm. Scale bar = 20 μm.

Supplementary Movie 5. Reversible changes in cell size through thermal control of meltITSN1-37. Cells expressing meltITSN1-37 were cultured at 41°C for 24 hours prior to imaging. Upon lowering the temperature to 37°C, cells showed rapid expansion in size, which could be toggled over multiple rounds of heating and cooling. Time is hh:mm. Scale bar = 20 μm.

Supplementary Movie 6. Temperature-inducible apoptosis using meltCasp1-37. HEK 293T cells transiently expressing meltCasp1-37 were exposed to either maintained 38°C or cooled to at 34°C.. Cells cooled to 34°C showed morphological changes associated with apoptosis, increased AnnexinV staining, and detachment from the plate. Time is hh:mm. Scale bar = 40 μm. meltCasp1-37 is shown in green while Annexin-V-647 is shown in magenta.